(NASA-CR-175618) RESEARCH IN PLANETARY STUDIES AND OPERATION OF MAUNA KEA OBSERVATORY Semiannual Progress Report, Jan. - Dec. 1984 (Hawaii Univ., Honolulu.) 61 p HC A04/MF A01 CSCL 03A G3/89
N85-23460
Unclas
14702

UNIVERSITY OF HAWAII

INSTITUTE FOR ASTRONOMY

2680 Woodlawn Drive

Honolulu, Hawaii 96822

NASA GRANT NGL 12-001-057

SEMIANNUAL PROGRESS REPORTS #28 and #29

Donald N. B. Hall, Principal Investigator

For the Period

January-December 1984

TABLE OF CONTENTS

		Page
I.	PERSONNEL	3
II.	THE RESEARCH PROGRAMS	4
	A. Highlights	4
	B. The Major Planets	5
	C. Satellites	18
	D. Asteroids and Comets	37
	E. Related Research Activities	55
III.	OTHER TOPICS	57
IV.	BOOKS AND PAPERS PUBLISHED OR SUBMITTED IN 1984	58
	A. Published	58
	B. Submitted or in Press	59

I. PERSONNEL

This report covers the period January-December 1984. Scientific personnel engaged in planetary research who were supported fully or in part by this grant during the report period area as follows:

D. P. Cruikshank	D. Morrison	C. B. Pilcher
W. M. Sinton	J. Goguen	D. J. Tholen
J. S. Morgan		

In addition, graduate students A. Storrs, H. Hammel, and J. Piscitelli received salary support on research assistantships. Undergraduate students W. Tittemore and K. Uchida were also employed to assist with the scientific projects.

II. THE RESEARCH PROGRAMS

A. HIGHLIGHTS

1. Acquisition and analysis of the first potassium images of the Io torus.
2. Determination, through analysis of the lightcurve, of the rotation period of Pluto as 6.38726 ± 0.00007 days (synodic), the most precise value yet obtained.
3. Correlation of Io torus emissions with volcanic outbursts on the satellite.
4. Significant improvements in the orbit of Pluto's satellite Charon, permitting more accurate predictions of the occultations and transits.
5. Discovery of an outburst on Io from observations at 3.8 and 4.8 μm.
6. Discovery of polarized thermal emission from Io, and the determination of the location of three thermal events (volcanoes) from the polarimetry.
7. Study of sodium tetrasulfide in connection with the composition of the surface of Io, particularly in terms of the satellite's surface variegation and the absence of thermally induced color phenomena during satellite eclipses.
8. Preliminary studies of liquid nitrogen/methane mixtures with gamma irradiation, in connection with Triton and Pluto.
9. Development of a theory of planetary surface photometry based on the assumption of isotropic multiple scattering.
10. Photometry of Titania, Oberon, and Triton, giving phase functions for the Uranian satellites similar to asteroids, but for Triton a value more consistent with an atmosphere or a high-albedo non-regolith surface.
11. Photometry of certain asteroids at near-zero solar phase angles.

12. Completion of a program to perform numerical integrations of Goguen's isotropic multiple scattering photometric function over surfaces of bodies of arbitrary shape and rotation curves.
13. Observations of several near-Earth asteroids, in particular 1983 TB, in infrared as well as visual wavelengths, in pursuit of the problem of the interrelationships between comets and asteroids.
14. Photometric and CCD observations of comet P/Halley with the 2.2-m telescope.
15. Study of the distribution of dust in the coma of comet IRAS-Araki-Alcock (1983d) from CCD images made with the 2.2-m telescope.
16. Determination of the temperature of comet IRAS-Araki-Alcock (1983d) from infrared photometry at several wavelengths with the NASA IRTF.
17. Continued study of the ice/dust systematics in the outer solar system bodies.

B. THE MAJOR PLANETS

1. Lightcurve of Pluto

Thlolen completed analysis of extensive photometric observations he made of Pluto at the University of Arizona between 1980 and 1983. A model was constructed that accurately describes the brightness variation with rotation, phase angle, and time. A more precise value for the rotation period of 6.38726 ± 0.00007 days was found; the small uncertainty on the period permits, for the first time, a distinction to be made between the synodic and sidereal rotation periods. The period quoted above reflects the synodic value; the sidereal value is 6.38755 days.

The rotational variation was found to be adequately described by a second-order Fourier fit. The physical interpretation of the result is that

Pluto's surface can be crudely described by the presence of two regions of lower albedo, approximately located diametrically opposite each other.

The slope of the phase function between 0.5 and 2.0 degrees was found to be 0.037 ± 0.002 mag/deg. This value represents a very shallow opposition effect, consistent with the high albedo estimates for Pluto's surface. Knowledge of this value will be invaluable when combining observations of eclipse events made at different phase angles (see below).

The secular fading of Pluto (due to the changing aspect of Pluto as it orbits the sun) was found to be 0.006 mag/year, on the average, between 1980 and 1983, roughly half the rate of fading found between 1955 and 1980. Thus we can conclude that more dark material is still coming into view in the immediate vicinity of Pluto's far pole.

2. Magnetospheres

Morgan and Pilcher are concluding a two-year CCD imaging study of optical and near-infrared emissions from the Io torus. The torus is the dominant feature of Jupiter's inner magnetosphere and is a highly dynamic entity. In the absence of new spacecraft data, ground-based imaging of the torus emissions has become our primary source of information concerning the temporal behavior of the torus plasma. In addition, it remains our most reliable source of information on the global, spatial distribution of torus plasma. In 1984 Morgan and Pilcher obtained 136 images of the plasma torus, 32 nearly concurrent images of Io's neutral sodium cloud, and the first images of Io's neutral potassium cloud. The plasma images include interleaved measurements of emission from [S II] $\lambda\lambda$6731,6716 and from [S III] λ9532. Through inter-comparisons of these images and comparisons with a similar inventory of images acquired in 1983, we are attempting to characterize and identify the processes which are responsible for the temporal variability of the torus.

In order to understand what physical plasma characteristics are implied by our data, and to distinguish temporal variations from variations caused by the rotation of the torus, we have constructed a three-dimensional model of the spatial distribution of torus plasma. We have computed such a model to match a sequence of images obtained on a single night in June 1983. The model enables us to invert our observed line intensities into physical plasma characteristics. We have used the model to identify features in this image sequence which are caused by the rotation of plasma "clumps" into and out of the image field of view. We are also using the model to help us determine whether observed differences between the east and west torus ansae are due to geometry or to intrinsic changes in the plasma. It has been suggested that temperatures and densities in the torus vary as a function of local time. Higher densities and temperatures are expected when the plasma is to the west of Jupiter. Owing to the Jovi-centric declination of the earth, the optical depth along a line of sight through a given eastern torus volume-element is different than when that element is observed to the west of Jupiter. The model enables us to account for this difference in geometry when comparing eastern and western torus images.

Figure 1 compares our model calculations with the corresponding 12 June 1983 torus images. The contour levels of the model calculations are identical to those of the corresponding images. In this figure the peak [S II] intensity in the "edge-on" image is approximately 2 times greater than that in the "open-ring" image. The figure shows that the model calculations do not yet match many details in the observed distributions, but the overall agreement is good.

Figures 2, 3, and 4 show the radial and longitudinal distribution of ions and electrons in the model. The model parameters between approximately 30°

Comparison of Models and Data

12 June 1983

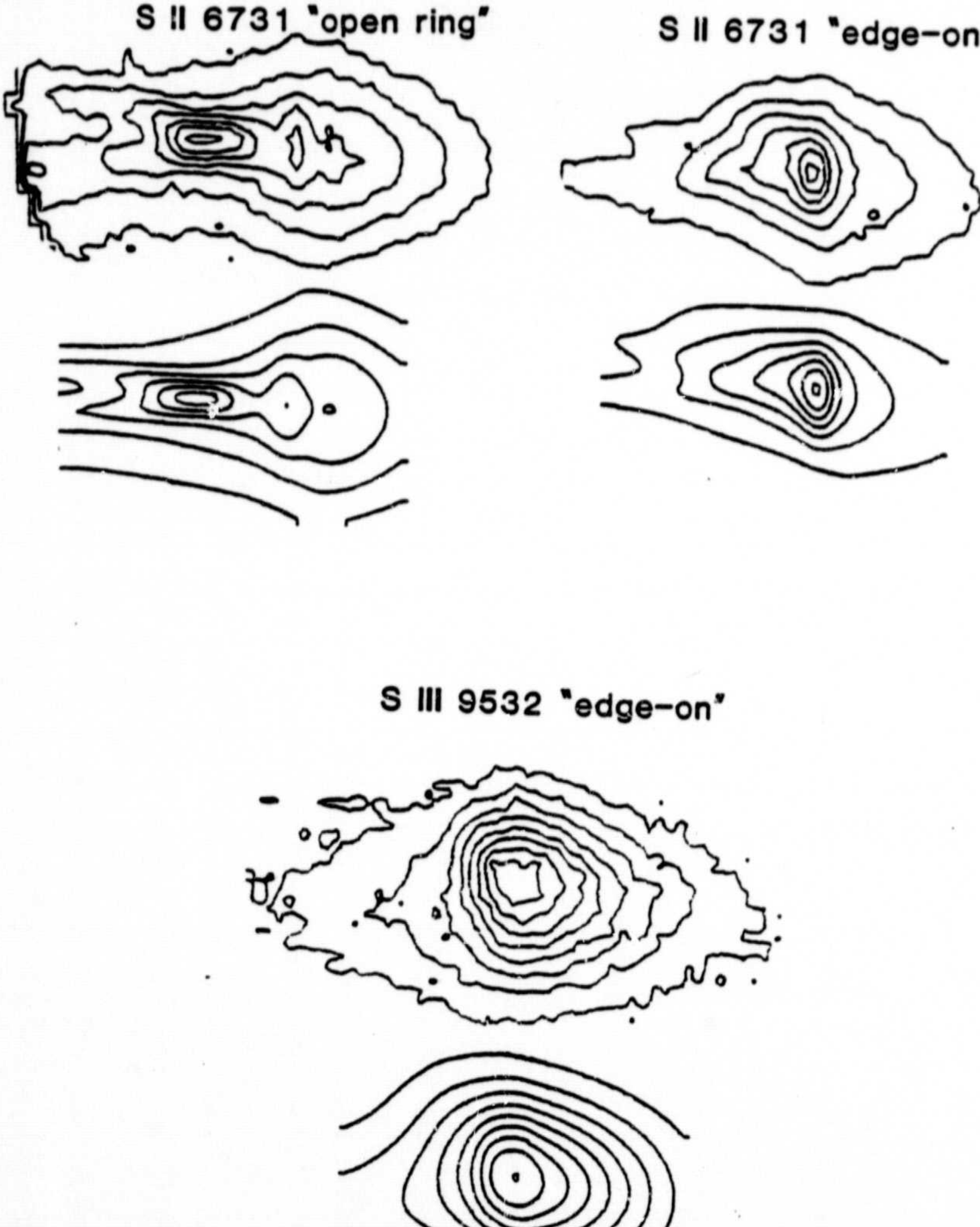

Fig. 1

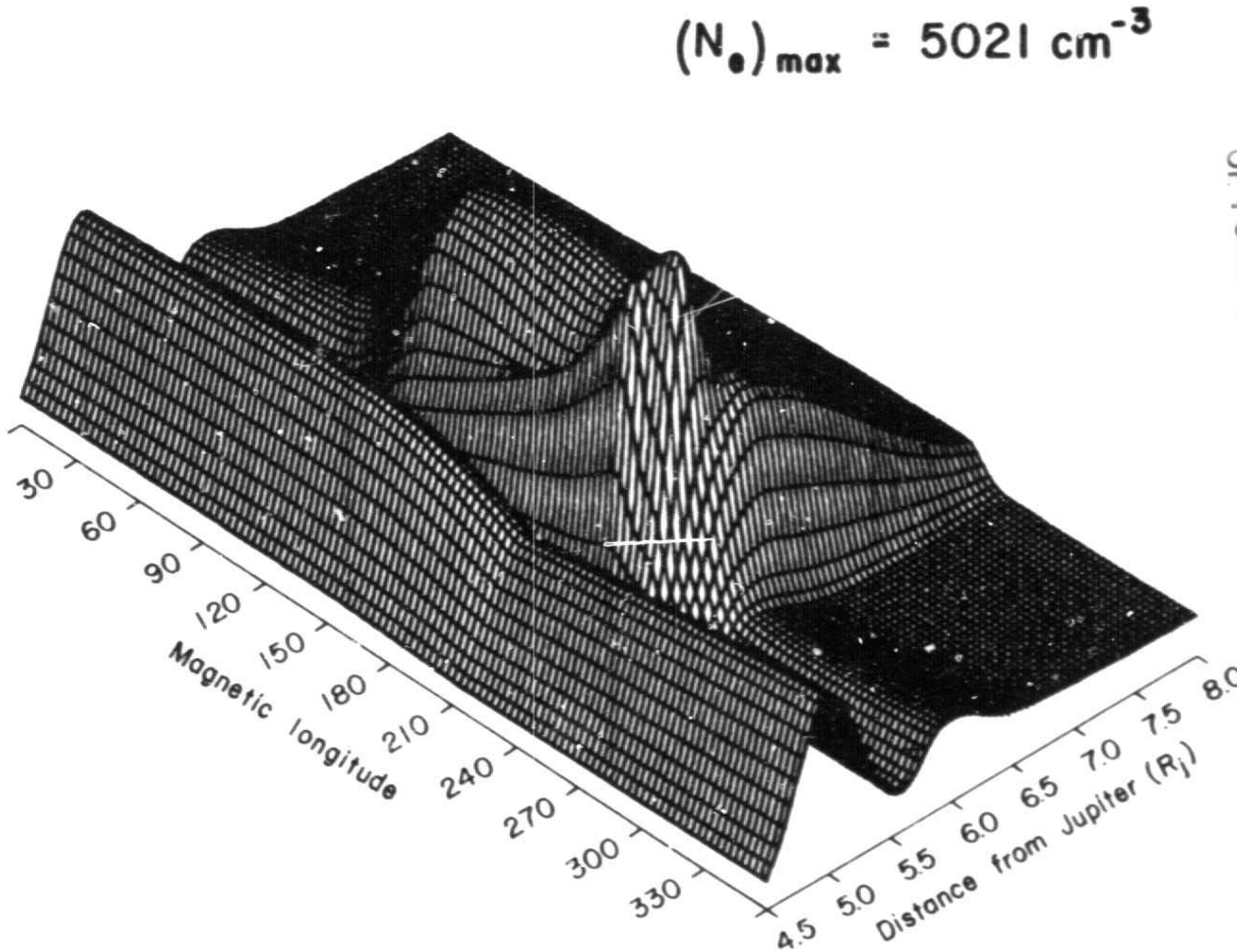
$(N_e)_{max}$ = 5021 cm^{-3}
30
60
90
120
150
180
210
240
270
300
330
Magnetic longitude
4.5
5.0
5.5
6.0
6.5
7.0
7.5
8.0
Distance from Jupiter (R_J)

Fig. 2

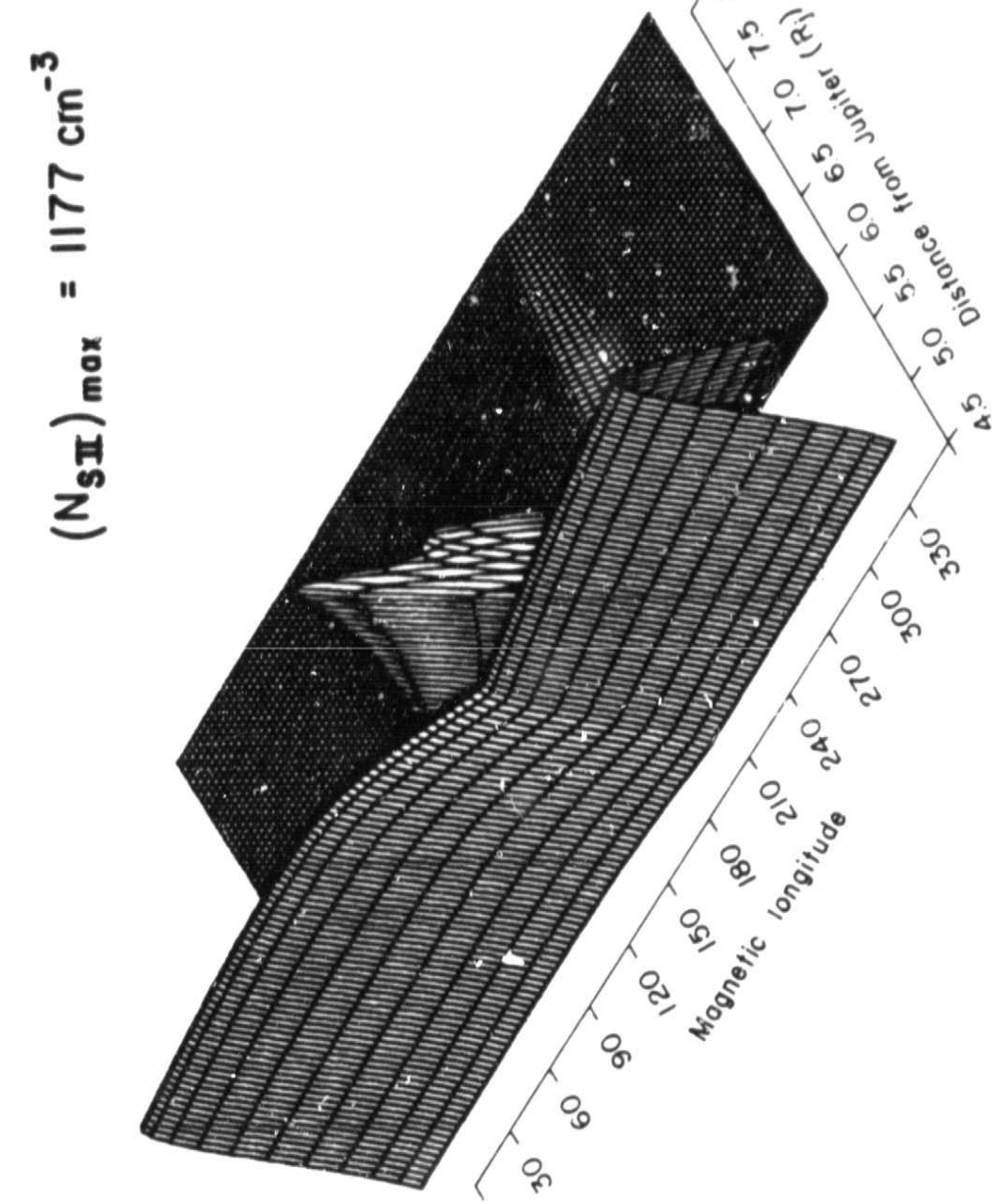
$(N_{SII})_{max}$ = 1177 cm^{-3}
Distance from Jupiter (R_J)
4.5 5.0 5.5 6.0 6.5 7.0 7.5 8.0
Magnetic longitude
30 60 90 120 150 180 210 240 270 300 330

Fig. 3

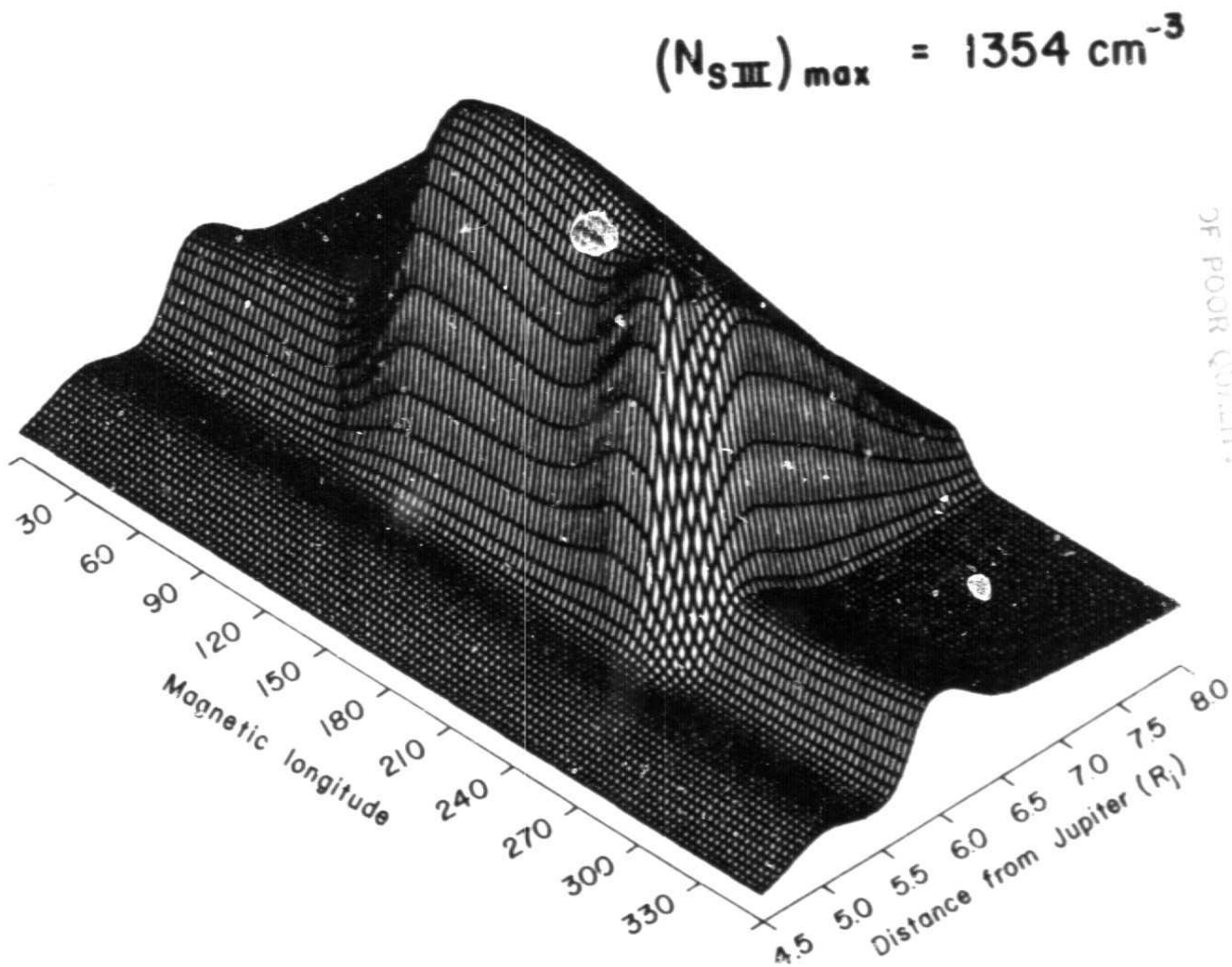
$(N_{S\,III})_{max} = 1354\ cm^{-3}$
30
60
90
120
150
180
210
240
270
300
330
Magnetic longitude
4.5
5.0
5.5
6.0
6.5
7.0
7.5
8.0
Distance from Jupiter (R_J)

Fig. 4

and 80° longitude, a region in which no images were obtained, were interpolated. The model indicates that the torus densities can vary by a factor of two within 5-10° of magnetic longitude. It indicates that in June 1983 density variations were primarily responsible for the observed longitudinal variations in torus brightness. However, variations in the torus ion mixing ratios were also evident. Near the density peak at ~230° the model S II and S III mixing ratios are ~0.15 and ~0.25, respectively. Near 100° the model S II and S III ratios are ~0.03 and ~0.35. Thus it appears that high S II mixing ratios are associated with the regions of high torus densities. This is evidence that within the high density region is a localized source of torus plasma.

The model does not yet give a good fit to the observed inner-torus emissions, but from the modeling efforts to date it is clear that the longitudinal variations near 5.0 R_J were much smaller than those in the outer torus. The current models have shown that the inner-torus emission brightness must vary by >25% as a function of longitude in order to fit the image data. The dependence of brightness on longitude in the inner torus is thus more complex than indicated in Figures 2 through 4. The observed variations may be caused by density variations. Alternatively, at the low temperatures characteristic of the inner torus, variations in electron temperature could also be responsible.

Figure 5 shows a comparison of [S II] images taken on 12 June 1983 with [S II] images taken two days earlier. This comparison presents strong evidence that the torus plasma near 5.7 R_J was lagging ~2% behind corotation at the time of these observations. In these images, the sharp decrease in plasma density with increasing longitude near 230° (see Figures 2 and 4) can be seen as an intensity "clump" that rotates into and out of the field of

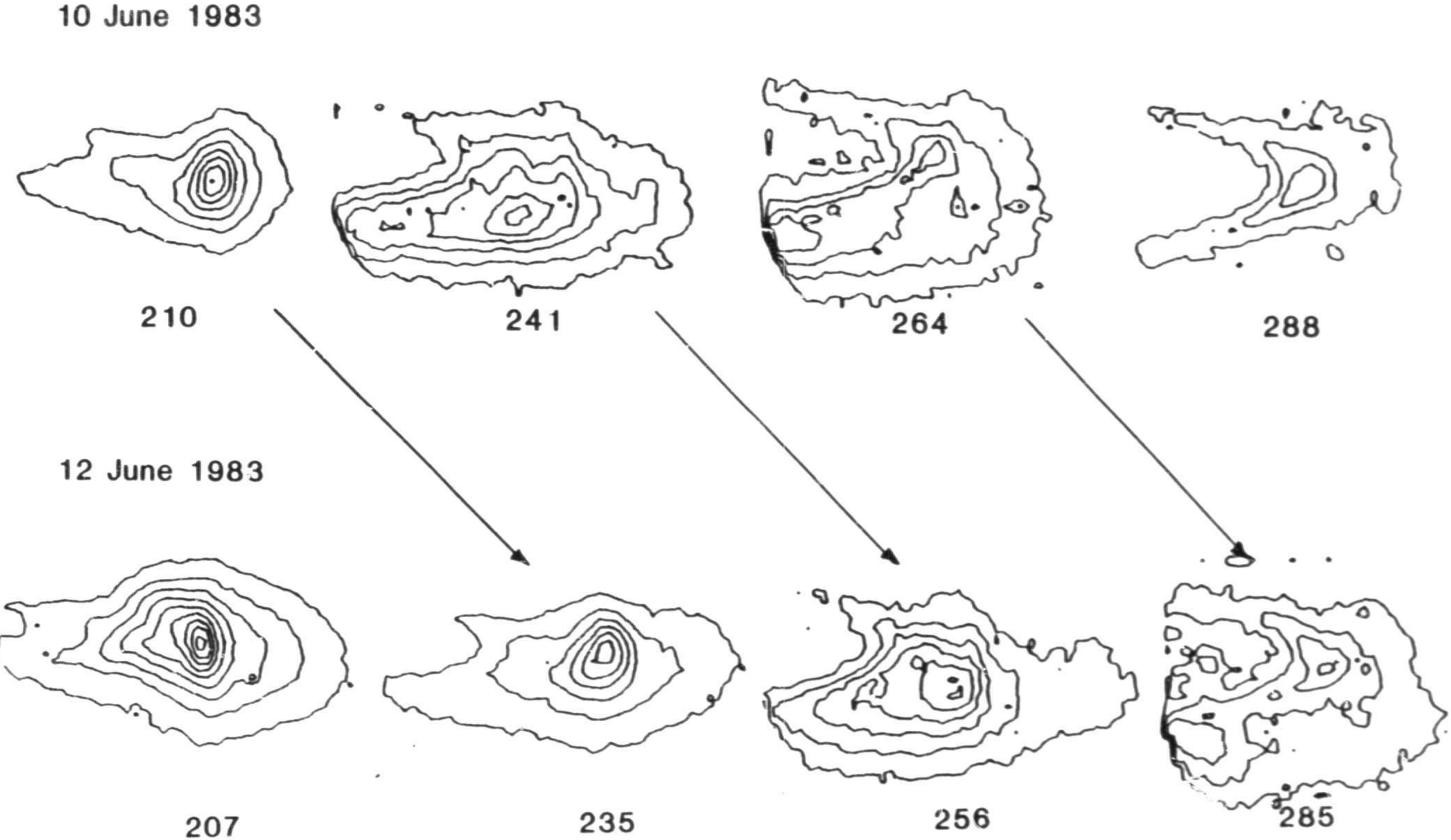

Fig. 5

view. In Figure 5, when this clump is near the torus ansa (10 June, longitude 241°; 12 June, longitude 256°) it appears as a radial extension of the torus. When the torus has rotated to a more "open-ring" configuration and the clump is near the edge of the field of view (10 June, longitude 264°; 12 June, longitude 285°), it appears as a "knot" of bright emission in the lower arm of the ring. Owing to the strong brightness variation with longitude, the location of the edge of this clump can be determined to within ~3° longitude in images where it appears away from the torus ansa. We have found that over a two-day period the edge of this clump shifted ~20° toward higher longitudes, implying ~2% subcorotation of the torus plasma. A comparison of the images acquired on 10 June at an ansa longitude of 288 and 12 June at a longitude of 285 confirm that the clump did indeed drift in magnetic longitude. Other images taken on the two nights at various longitudes are consistent with a ~10° per day drift rate. Figure 5 shows a subset of the images available for comparison.

Figures 6, 7, and 8 compare images taken to the east and west of Jupiter at similar ansa longitudes. These figures show strong evidence that a local-time (east-west) asymmetry exists in the torus. These images represent an important confirmation of the east-west asymmetry that we reported earlier in spectroscopic measurements. To the west of Jupiter, the torus is found to be 34 ± 3% brighter than to the east. The peak brightness (in Rayleighs) and the ansa longitude of each image are labeled on the figures. In Figures 6 and 7 the eastern images were obtained on 25 June 1984 and the western images were obtained on 26 June 1984. Figure 8 illustrates that the observed asymmetry is not caused by temporal changes in the nebula. The images in Figure 8 were acquired on the same night on 17 June 1984 only 5 hours apart. We are currently using models similar to the one described above to study the details of the observed asymmetry.

East-West Intensity Asymmetry

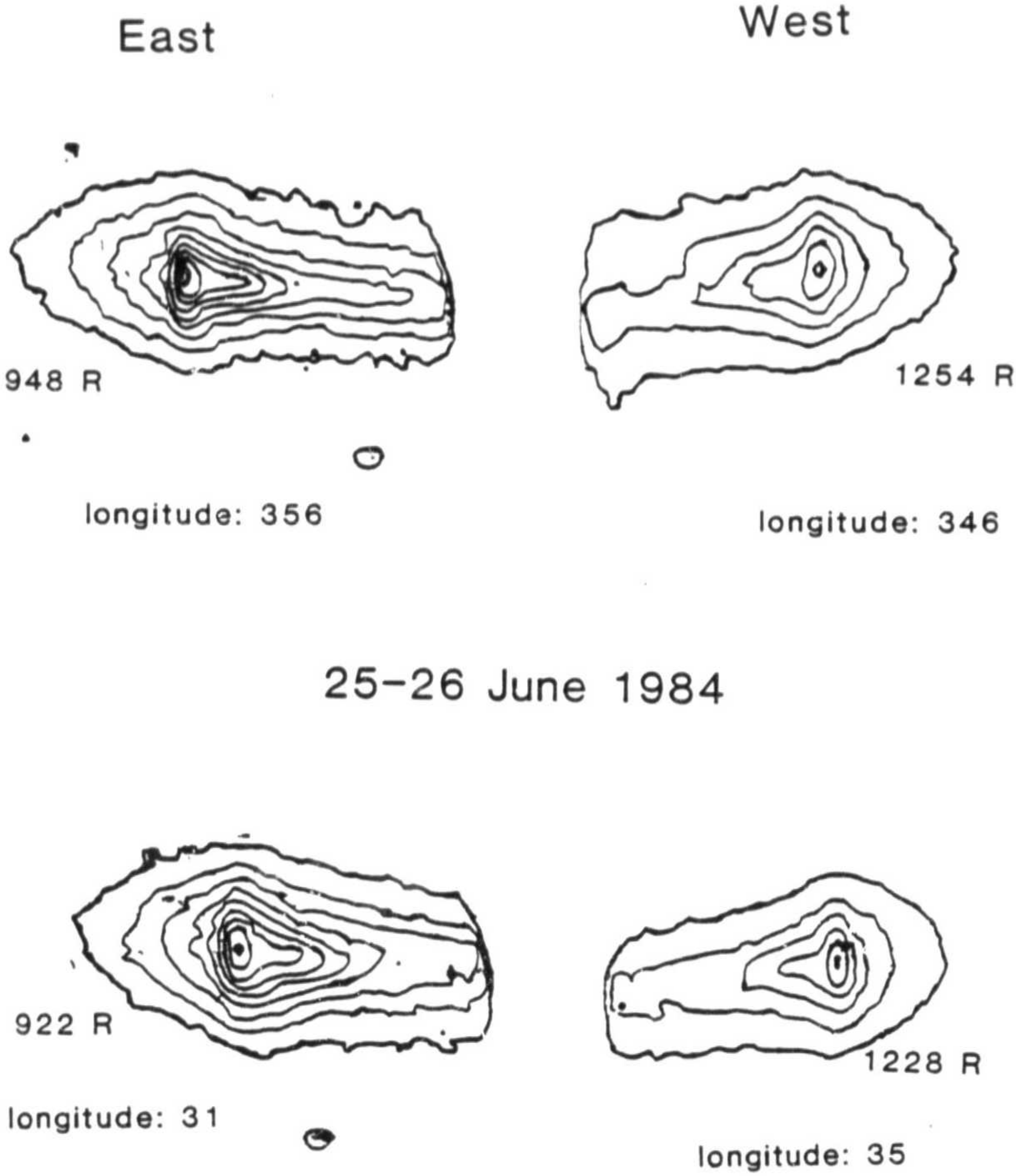

Fig. 6

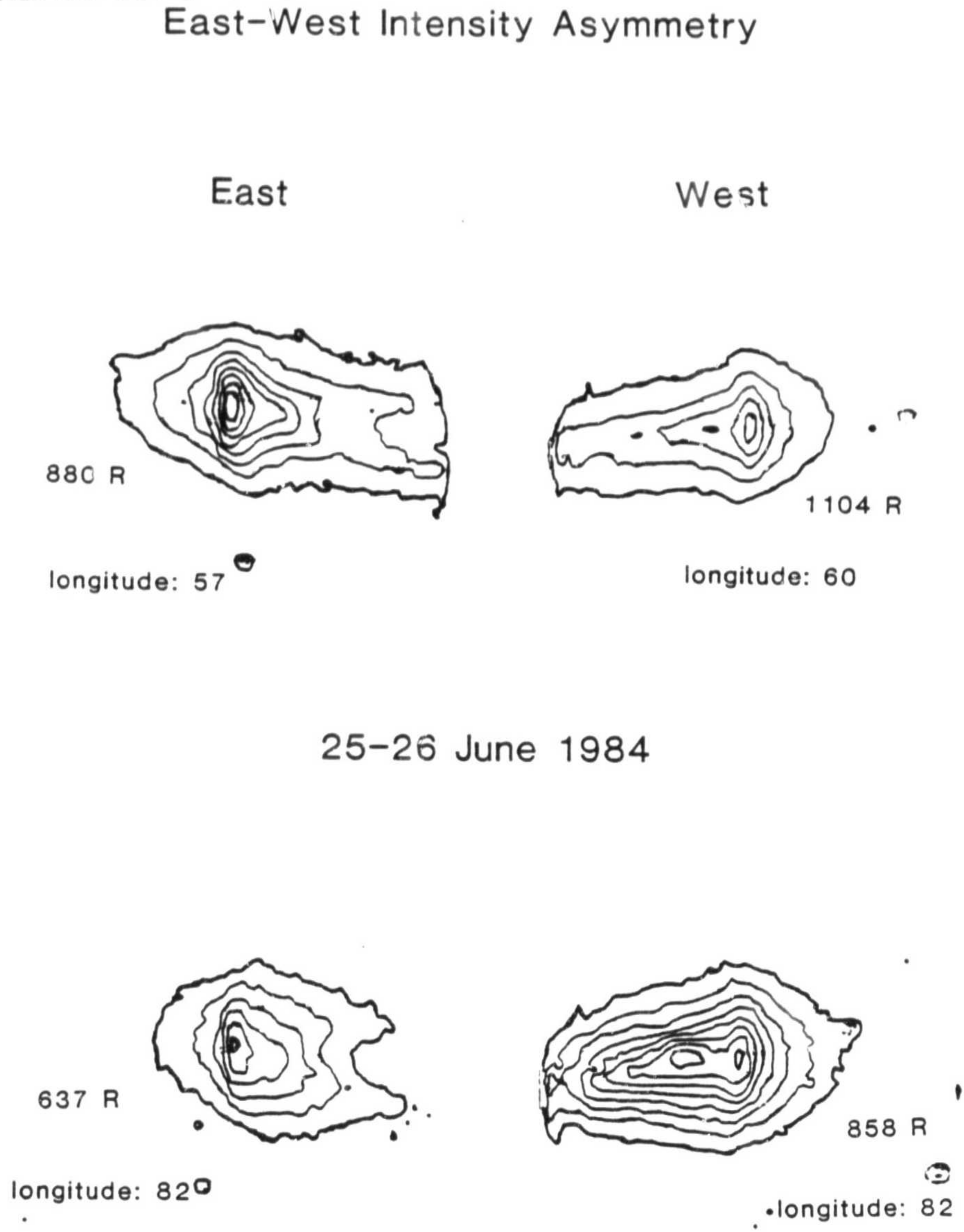
East-West Intensity Asymmetry
East
West
880 R
1104 R
longitude: 57
longitude: 60
25-26 June 1984
637 R
858 R
longitude: 82
longitude: 82

Fig. 7

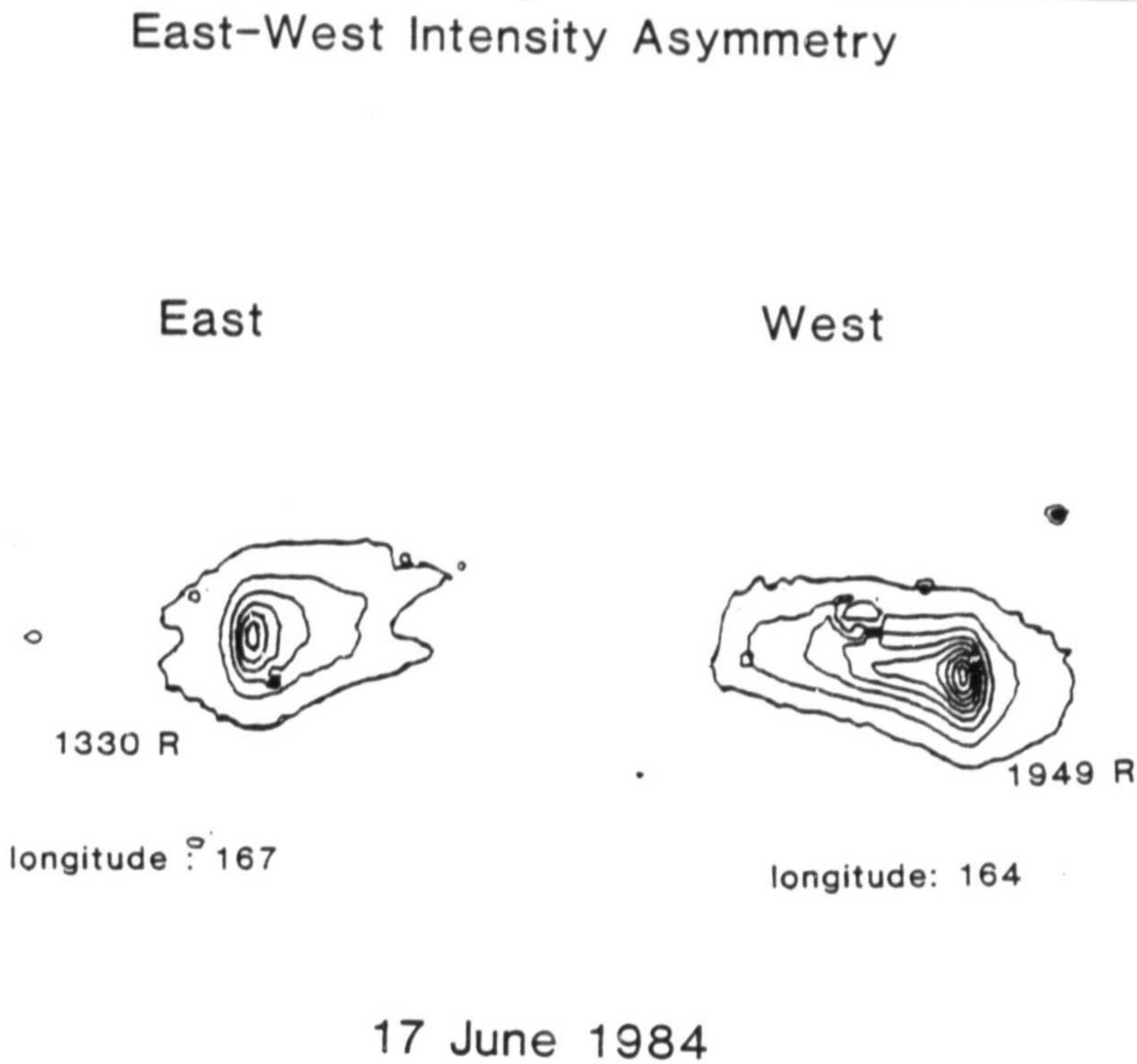
East-West Intensity Asymmetry
East
West
1330 R
1949 R
longitude : 167
longitude: 164
17 June 1984

Fig. 8

Finally, we now have data which may help us to understand relationships between volcanic activity on Io and temporal changes in the torus. Sinton and Goguen's measurements of the 4.8 μm flux from Io indicates that Loki experienced a substantial eruption in 1984. The eruption began in early June, peaked in mid- or late-July, and was substantially diminished by mid-September. We have torus images in mid- and late-June which show bright [S II] and [S III] torus emission (~1600 and 2500 Rayleighs, respectively). In mid-August we have images that show these same torus emissions to be 4 to 5 times dimmer. The implication appears to be that bright torus emission occurs during the initial phases of a volcanic outburst on Io. This will be the subject of future studies of our data. It is our hope that future observations will allow further study of the relationship between the torus and Io's volcanic activity.

C. SATELLITES

1. Photometry of Pluto/Charon Mutual Events

High time resolution observations of the Pluto system were attempted by Tholen on six nights when mutual events were predicted to occur. Three nights yielded excellent data but no events were seen. The data remain quite useful, however, serving to determine reference uneclipsed lightcurves from which accurate depths can be measured once events commence.

2. Determination of the Orbit of Charon

Prior to the beginning of the 1984 eclipse "season", the predicted times of events still had uncomfortably large uncertainties associated with them. In order to rectify this situation, Tholen collected eighteen available speckle interferometric observations of the system and performed an orbit improvement. The orbital period was found to be in excellent agreement with the rotation period found from the lightcurve, providing experimental evidence for synchronous rotation/revolution. The improved values for the period and the orbital radius permitted an improved mass determination to be made. The total mass was found to be 7.0 ± 0.5 E-9 solar masses. Once eclipse observations yield accurate diameters for the two bodies, the first reliable density determinations can be made.

Although the new orbit represents a significant improvement over the previously available orbit, the results are being taken cautiously due to the presence of systematic residuals. Analysis of the data continues in an effort to understand and possibly compensate for the systematic effects.

3. Io

Sinton and Tittemore have continued monitoring Io at 3.8 and 4.8 μm. This program has been especially valuable this year for a moderate outburst that lasted for several months was discovered on the trailing hemisphere of Io. From the speckle interferometry work of Howell and from the polarization studies of Goguen and Sinton, this outburst was identified as a renewed vigor in the eruption of the Loki volcano. From measurements from April through September, it was found that the activity began in mid-June, peaked in mid-July, was waning by mid-August, and by September was nearly back to the April level. A thermal emission enhancement of the nominal "geometric albedo" was observed at both 3.8 and 4.8 μm; at M the peak value was 1.3, which may be compared to the usual 0.8 to 0.9. Such a long duration outburst has not been seen before.

Goguen and Sinton measured, for the first time, the polarization of the thermal emission from Io at 4.8 μm using the IRTF and its wire grid polarimeter. Polarization of the emission from the volcanoes was expected because thermal radiation from a dielectric surface (lava for example) is polarized as a consequence of Fresnel reflection laws combined with Kirchoff's law relating to the emissivity (Figure 9). In acvance of the observation, models were constructed that gave the variation of the first three Stokes parameters with rotation of a single hot spot and a mixture of hot spots across the surface of Io. The observations gave a maximum observed polarization of 1.6% which varied down to near zero as the observed spot crossed the central meridian. The plane of polarization also rotated in accordance with the theory, and the precise relationship with Io's rotation gives an accurate determination of the latitude and longitude of the spot. From modeling the observations and using more than one spot, it was possible to fit all three Stokes parameters within their measurement errors for the 22 sets of data obtained on 8, 9, and 10 July 1984. Three spots suffice, but there are two possible solutions summarized in Table 1.

Table 1. Best Fit Parameters for Three Spots

Sol'n	n	p	Lo_1	La_1	A_1	Lo_2	La_2	A_2	Lo_3	La_3	A_3
1	1.52	0.84	289	19	2700	72	6	1250	322	-13	1400
2	1.52	0.84	311	-1	2630	71	6	1220	277	27	1430

The meaning and units of the quantities in Table 1 are: n, index of refraction of the lava at 4.8 μm; p, geometric albedo of Io with no contribution from volcanic emission; Lo, west longitude in degrees of the spot numbered by the subscript; La, latitude in degrees of the spot of subscript number; and A, area of the spot in square kilometers corresponding to the subscript. The areas, but none of the other parameters, are contingent upon our assumption of 450 K for all spot temperatures. For other temperatures, the areas will scale inversely as the blackbody function at that temperature and the wavelength

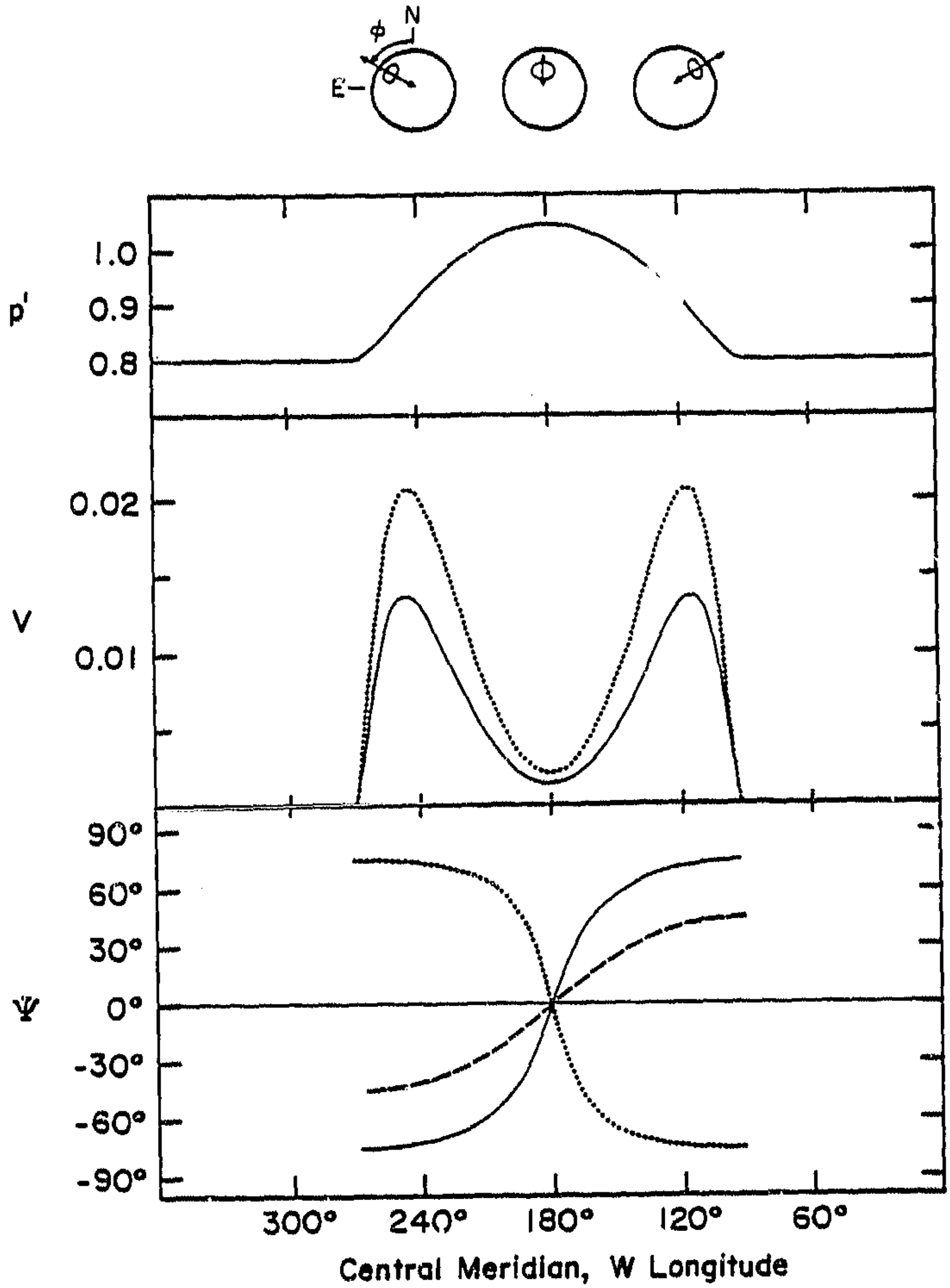

Fig. 9 The variation of flux and linear polarization with orbital longitude due to the presence of a single "standard" hot spot of area 2000 km^2 (T = 450 K) located at 180 W, 15 N on a model planet with n = 1.5 and a true geometric albedo of 0.8. The schematic above the figure illustrates this spot and its apparent change for three orientations. The arrow length is propotional to the degree of polarization and phi is the position angle of the spot on the disk. In each frame of the figure, the solid line is the signature of this "standard spot" and the broken lines show the changes in this signature if *one* of the parameters is varied from the standard configuration. Top: The "effective geometric albedo", p' (see text). Middle: The degree of linear polarization, V. (Dotted line, n = 1.8) Bottom: Position angle of linear polarization, psi. (Dashed line, latitude 45 N; dotted line, latitude 15 S)

4.8 μm. We prefer the first solution given in Table 1 because it gave a slightly better fit, and because the spot numbered 1 is in better agreement with the position of the Loki volcano. Formal errors for latitude and longitudes are rarely in excess of 2°. However, systematic errors may cause larger uncertainties. In comparing these positions to the Voyager map of Io, one should remember that there may be as much as 5 to 10° error in the map relative to the I.A.U. system of coordinates. Also the positions given here may be confused by the presence of unaccounted for hot spots on Io. The fit of the model curves to the observed data for the first solution is shown in Figure 10.

Hammel has completed the reduction of the infrared curves from the lunar occultation of Io that occurred on 2 April 1983. The data were obtained in a coordinated program, organized by Sinton, at the IRTF, Ukirt, the 5-m Hale telescope, and the 4-m Mayall telescope. The observers, besides Sinton, were E. Becklin, I. Gatley, K. Matthews, S. Ridgway, and Goguen and Hammel who made supportive visual wavelength observations at the UH 2.2-m telescope. No discrete hot spots at 3.8 μm (the wavelength used for the IR observations) were found by any observer. The 3σ limit for the area of a 450 K spot set by these observations is 3400 km^2. The region observed is the hemisphere centered on longitude 65°, which is the most inactive region of Io. Thus the observations are not in disagreement with the previously mentioned polarization observation of a 1250 km^2 spot at longitude 72° in 1984. The reasons for the insensitivity of the lunar occultation observations are that the entire phenomenon transpired in 4 seconds and the choice of 3.8 μm which was dictated by the rapidity of the event. If, however, the occultation had been of the trailing hemisphere, the Loki volcano probably would have been detected. A conclusion that can be drawn from the observations is that a

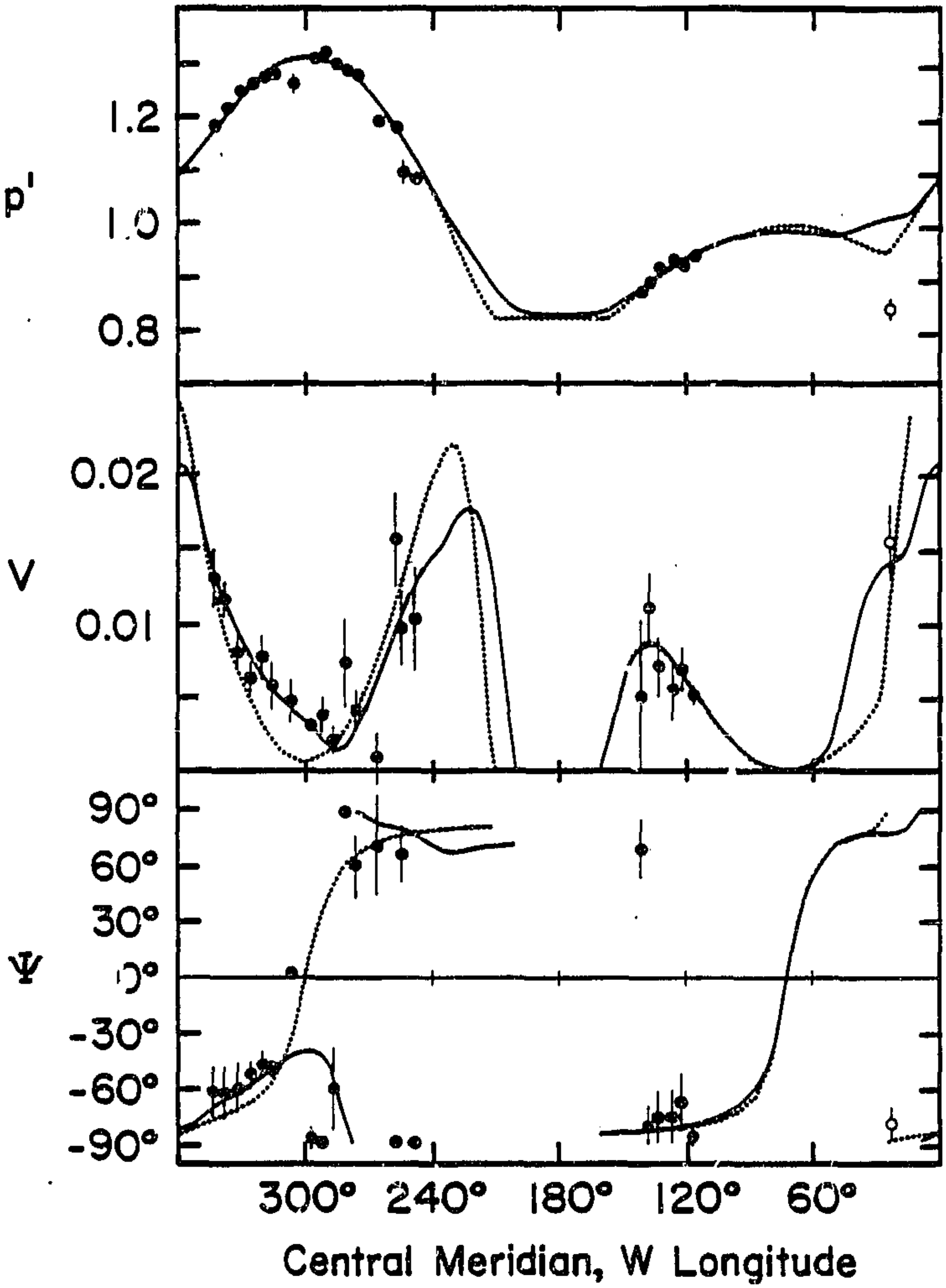

Fig. 10. Observations (filled points) and the best two-spot (dotted lines) and three-spot models (solid lines, see Table I.) of Io's 4.76 um flux and linear polarization on 8, 9 and 10 July, 1984 UT. The open points are from 13 August, 1984 and were not included in the fit due to their non-simultaneity with the other data. (See Fig. 9.) Top: "Effective geometric albedo", p'. Middle: Degree of linear polarization, V. Bottom: Position angle of linear polarization, psi.

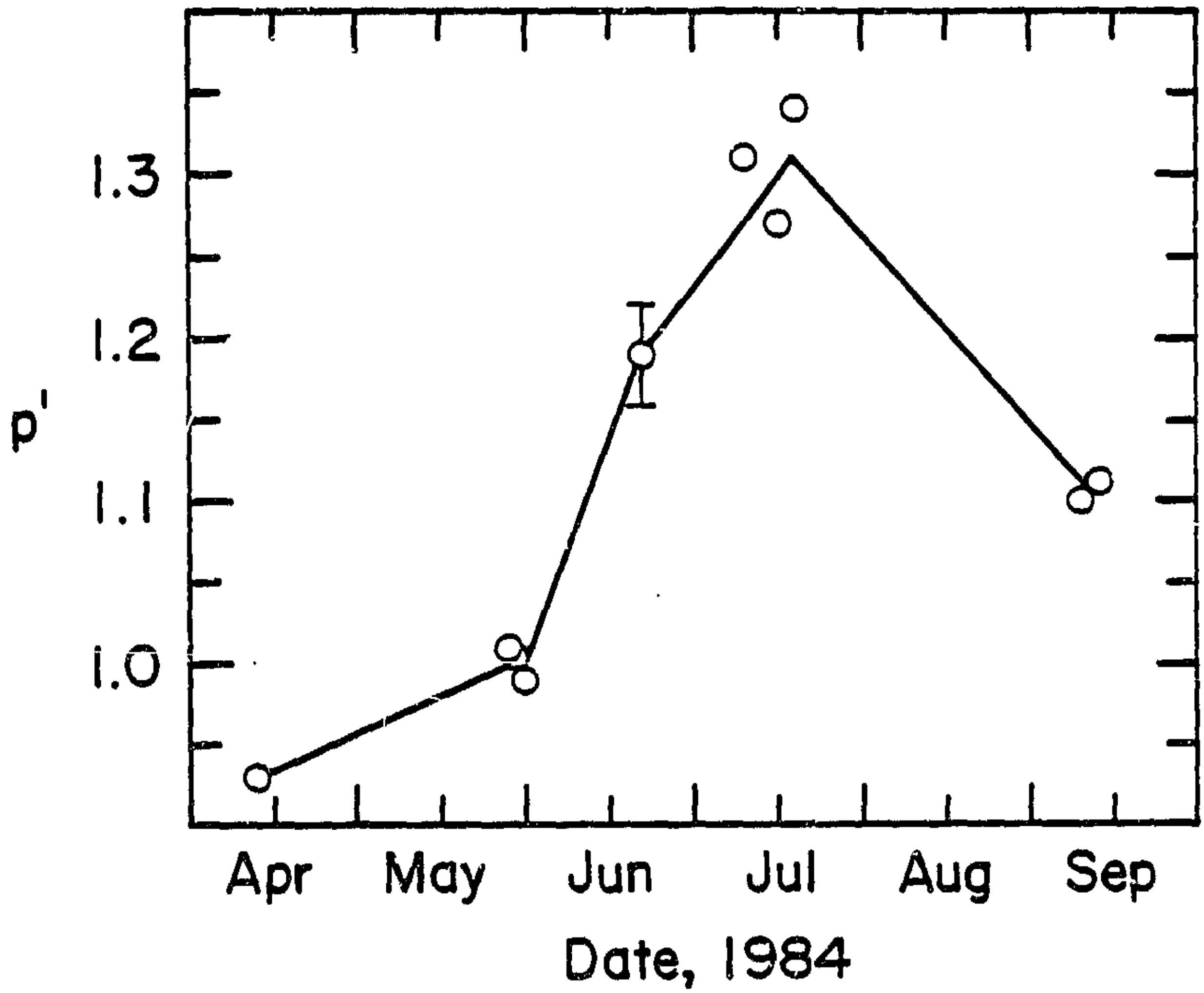

Fig. 11. The flux history of the Loki eruption during 1984. Each observed flux with Loki visible has been corrected to obtain the "effective geometric albedo" with Loki on the central meridian. The Loki flux varies by nearly a factor of 4 at 4.76 um during this period. If the hot spot flux were "switched off", p' = p = 0.8.

uniform disk is a good model for the reflected sunlight. Thus there is no appreciable limb darkening or brightening of Io at 3.8 μm.

4. Europa, Ganymede, and Callisto

Observations that have been made in the K, L', and M photometric bands (2.2, 3.8, and 4.8 μm) by Sinton and his collaborators since 1979 have been reduced by Tittemore. A total of 19 observations of Europa, 87 of Ganymede, and 79 of Callisto have been analyzed. Solar phase coefficients were determined in the K, L', and M bands for Ganymede and in the K and L' bands for Callisto. The orbital phase variations for Ganymede and Callisto are small at all three wavelengths. The geometric albedos for both are close to 0.25 at K and 0.1 or less at L' and M. The low values at the latter wavelengths are expected from the presence of water ice on their surfaces. The geometric albedos of Europa are: K, 0.19; L', 0.02; and M, 0.015. The very low albedos at L' and M are due to the nearly complete coverage by water ice. Because of the low albedo, Europa is a difficult object to detect at 4.8 μm, even with the IRTF.

5. Laboratory Measurements

The widely held belief in the abundant presence of elemental sulfur on Io's surface is now being questioned by a number of researchers. Some of the reasons for questioning the ubiquitous presence of sulfur are: a black sulfur lake at 450 K (e.g., Loki) would be boiling violently and would have to be more than 1 kilometer keep to remain very long; it is not possible to quench the colors of molten sulfur by radiative loss of heat as had been proposed; a thermal shift of the absorption edge of the S_8 molecule in posteclipse photometry by Hammel, Goguen, Sinton, and Cruikshank was not found, thus setting a 50% upper limit for surface coverage by sulfur; and recently, the polarization determination of a refractive index of 1.5 for the hot sp as opposed to the 1.8 index of sulfur. None of these arguments is conc. in eliminating sulfur, but taken together they give reason to examine other alternatives.

Sinton has been considering some other possible alternatives. Taking the cosmic abundance of nonvolatile chemical elements as a guide and particularly considering those elements that are known to be driven off of the surface of Io, viz. Na, S, O, and K; he examined the table of inorganic compounds for those that were yellow and which had higher melting points than allotropes of sulfur. This search led to the class of sodium polysulfides as possible constituents. Of these, sodium tetrasulfide, Na_2S_4, appears as a particularly good candidate in that not only is it yellow, but it has a melting point ~550 K. Sodium tetrasulfide is a better candidate than other sodium sulfides because it has a strong yellow color and it has the highest melting point with the exception of Na_2S, which is nearly white. A small amount of the compound was purchased; it is expensive. Some was also synthesized, which is a complicated process partly because it is very hygroscopic and reacts with water or air to form various sulfates. A whole battery of tests need to be run on Na_2S_4. Some simple tests have been made. When crystals of it are dropped into liquid nitrogen the yellow color barely fades. On the other hand, crystals of sulfur become a light cream color in nitrogen. Thus the thermal shift of the blue absorption edge is much less for Na_2S_4 than for S_8. However, heating Ha_2S_4, in a partial vacuum to exclude air, produced color changes to red and then to black as the melting point was approached. Upon cooling, the sample required several weeks to regain its yellow color. The conclusion which may be drawn is that the variety of colors seen on Io may be obtained with Na_2S_4 within the large color shift that would occur with sulfur on posteclipse warming.

Sinton sought to obtain an infrared transmission spectrum of Na_2S_4 but was temporarily thwarted by equipment breakdowns and the difficulty of handling samples.

6. Laboratory Studies of Nitrogen and Methane Mixture

A spectral feature attributed to liquid nitrogen has been detected on Triton (Cruikshank et al. 1984). With the presence of methane already firmly established (Cruikshank and Apt 1984), the surface colors and reflectance spectrum can be modeled in the laboratory. Cryogenic experiments involving liquid nitrogen as a solvent and methane as a solute have shown that methane has a reasonably high solubility (~83 grams/liter) in ℓN_2. (Delitsky, preprint). Irradiation by γ-rays, which simulate the galactic cosmic ray flux, produces a variety of organic chemicals which precipitate to the bottom of the container (Siderer and Sato 1975). A preliminary check of this result using commercial ℓN_2 with gaseous methane bubbled through and then irradiated at the Hawaii Research Irradiator did show a large yield of yellowish-white precipitate. However, due to the rapid oxidation of the sample, the presence of oxygen compounds was inferred. The next stage in the experiment was to build a distillation apperatus for the creation of high purity ℓN_2. Currently, the experiment is at the tertiary stage, where the high purity irradiated samples are being observed with the spectrogoniometer at the Planetary Geosciences Division at the University of Hawaii. Results are in progress.

7. The Isotropic Multiple Scattering Approximation and Its Application to Planetary Surface Photometry

Goguen (in collaboration with J. Veverka of Cornell) has developed an approach to the analysis of planetary (particulate) surface photometry that is based on the assumption of isotropic multiple scattering and should be applicable across an extended range of particle albedos, opacities, and separations. Although the basic equations reduce to Hapke's treatment of scattering from a particulate surface in the limit of large, opaque, closely spaced particles, it is shown in general that if the phase angle dependence of the photometric function is separable from the incidence and emission angle dependence, a generalized form of this same function should also apply to surfaces composed of transparent and/or well separated particles. This removes the restriction of application of this type of function to only surfaces of low albedo, and allows modeling of scattering from the icy, high albedo surfaces common in the outer solar system. This photometric function is defined in terms of an "effective particle albedo" parameter w and an "effective particle phase function" $f\alpha$. $f\alpha$ includes the effects of anisotropic scattering and (perhaps partial) interparticle shadowing and is determined empirically. One important consequence of this treatment is that the photometric function is fully determined in the lab by measurements of the surface normal reflectance, opposition limb-darkening and one intensity at each of a range of phase angles. For a homogeneous, spherical planet, the surface photometric function may be completely deduced from observations of the geometric albedo. The normal reflectance and the disk-integrated phase curve. Work is underway to find the w and $f\alpha$ most appropriate to asteroid and satellite surfaces for which suitable photometry exists. If the H-functions for isotropic scattering are approximated as linear in the cosine of their angular argument, a very simple form of the model function is obtained which is the sum of three terms: Lambert and Lommel-Seeliger components and a new term which is largest for high albedo surfaces near normal incidence and viewing. Simple expressions are derived for the geometric albedo, phase integral, Bond albedo and phase curve of a spherical planet whose surface scatters according to this photometric function. A first paper in this study has been submitted to Icarus and is currently under revision.

8. Photometry of Titania, Oberon, and Triton

Goguen, Hammel, and Brown have obtained V photometry of the two outer satellites of Uranus and Triton that covers the observable three degrees of phase angle. They find that Titania and Oberon have phase coefficients typical of asteroids observed at this geometry (0.1 mag/deg) but that Triton has a much smaller phase coefficient (0.03 mag/deg). This suggests that the Uranian satellites may have regoliths of opaque particles like the asteroids and are of low to moderate albedo. Possible explanations for Triton's small phase coefficient include an optically thick atmosphere or cloud layer, a high albedo surface or a non-regolith surface (e.g., an ocean). Observations at 0.06° phase angle show the 0.2 mag additional brightness surge reported in the IR by Brown. Orbital lightcurves are less than 0.1 mag amplitude for all three bodies. Oberon may be a few percent brighter at its southern elongation than at its northern. Additional observations not yet reduced should improve the determination of Oberon's orbital variation which, if confirmed, suggests that Oberon's orbit may not yet be tidally evolved to its final zero obliquity, synchronous state. A manuscript submitted to Icarus has been accepted.

9. Very Small Phase Angle Photometry of Solar System Surfaces

Goguen, Hammel, and Tholen have begun a project to determine the differences or similarities of the opposition effect among asteroid and satellite surfaces. A computer search generated a list of all asteroids approaching within 2° of opposition. Of these, the brightest and smallest phase angle objects were selected and V photometry obtained. Asteroids 10, 16, 21, 33, 79, 211, and 704 have all been observed at phase angles less than 1° and followed up at larger phase angles. In addition it was noted that Jupiter attained a phase angle of less than 0.1° and 3 color observations of all 4 Galilean satellites were obtained at opposition and at larger phase angles. This photometry will be analyzed using the isotropic multiple scattering photometric function (discussed elsewhere in this report) to define the $f\alpha$ function for different types of solar system surfaces at phase angles observable from earth. There should be sufficient very small phase angle (<0.5°) data to determine if the large surge of 0.2 mag in the last 0.5° of phase angle exhibited by the Uranian satellites is a unique phenomenon or a common one not observed for most objects because the very small phase angle geometry is only rarely attained.

10. Sulfur Allotropes on the Surface of Io

One of the intrinsic properties of sulfur allotropes is a temperature-dependent change in reflectivity. The surface of Io experiences temperature changes during eclipse which are sufficient to cause a detectable change in the spectral reflectivity of sulfur; thus, if the surface of Io is composed primarily of sulfur allotropes, a change in reflectivity should be observable during eclipse reappearance. We observed four eclipse reappearances during July and August of 1983 and saw no posteclipse brightening effects in filter bands selected for sensitivity to color changes in sulfur. Our model of the brightness change for yellow sulfur implies that this material covers less than 50% of Io's surface. Negative observations were also obtained with a filter chosen for the high contrast between SO_2 frost and the average albedo of the surface of Io at that wavelength. We conclude that no significant condensation of SO_2 occurred during these eclipses.

Figures 12 and 13 show the observations made in conjunction with this work. Figure 12 gives the 0.44 μm and 0.36 μm magnitudes, offset from the 0.71 μm magnitudes (upper curve in each set), by 0.6 and 1.2, respectively. Figure 13 shows the colors of the eclipse reappearances. For each night, the upper curve is the 0.44/0.71 μm color and the lower curve is the 0.36/0.71 μm color.

11. The Dark Hemisphere of Iapetus

Cruikshank continued his collaboration with J. Bell (PGD) on a spectrophotometric study of the dark hemisphere of Iapetus. This work was described in last year's report, but in this report year the paper was completed and submitted (to *Icarus*). The abstract of this paper follows:

Telescopic observations, laboratory simulations, and photogeological studies have been conducted to investigate the composition of the dark material on Iapetus and the reasons for its peculiar distribution. The results of our earlier studies (*Icarus* 53, 90-104) are confirmed and extended. Improved telescopic spectra of leading and trailing hemispheres were obtained over the 0.3-2.6 μm range. A mixing model was used to correct the leading-side spectral data for the presence of regions of bright terrain at both poles. The resulting true dark-unit spectrum is much redder in the visible and near-IR than previous uncorrected spectra, but gradually flattens near 2.0 μm. This unusual spectrum is reproduced with an intimate mixture of simulated meteoritic organic polymers (10%) and hydrated silicates (90%) which corresponds to an extension of the compositional trends in known carbonaceous meteorites toward lower formation temperatures. Structures in the dark/bright transition zone visible in the Voyager 2 images are inconsistent with an eruptive origin for the dark material; this zone is probably the region of grazing impacts of dust spiraling in from Phoebe. The dark material is

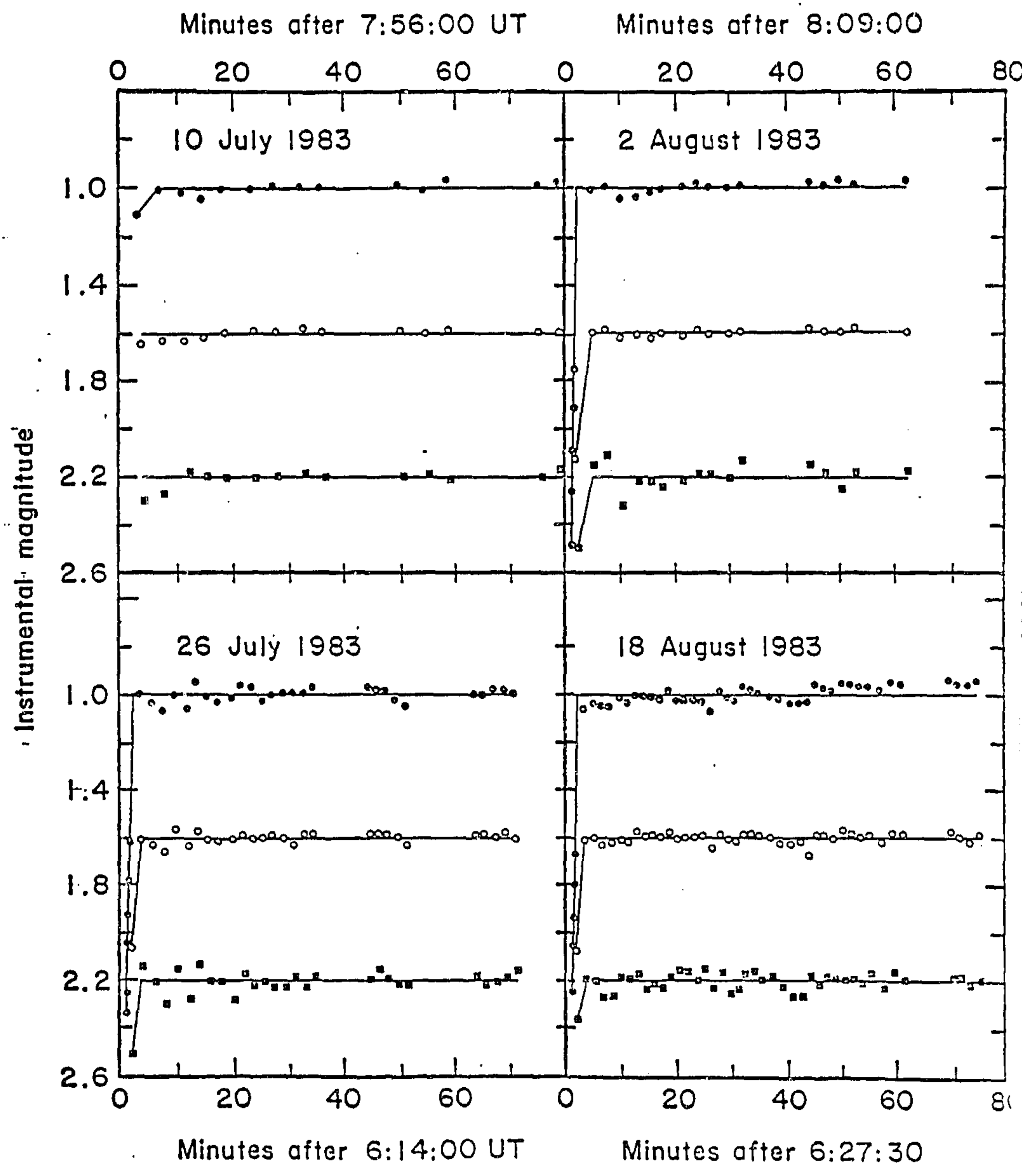
Minutes after 7:56:00 UT
Minutes after 8:09:00
0
20
40
60
0
20
40
60
80
10 July 1983
2 August 1983
1.0
1.4
1.8
2.2
2.6
Instrumental magnitude
26 July 1983
18 August 1983
1.0
1.4
1.8
2.2
2.6
0
20
40
60
0
20
40
60
80
Minutes after 6:14:00 UT
Minutes after 6:27:30

Fig. 12

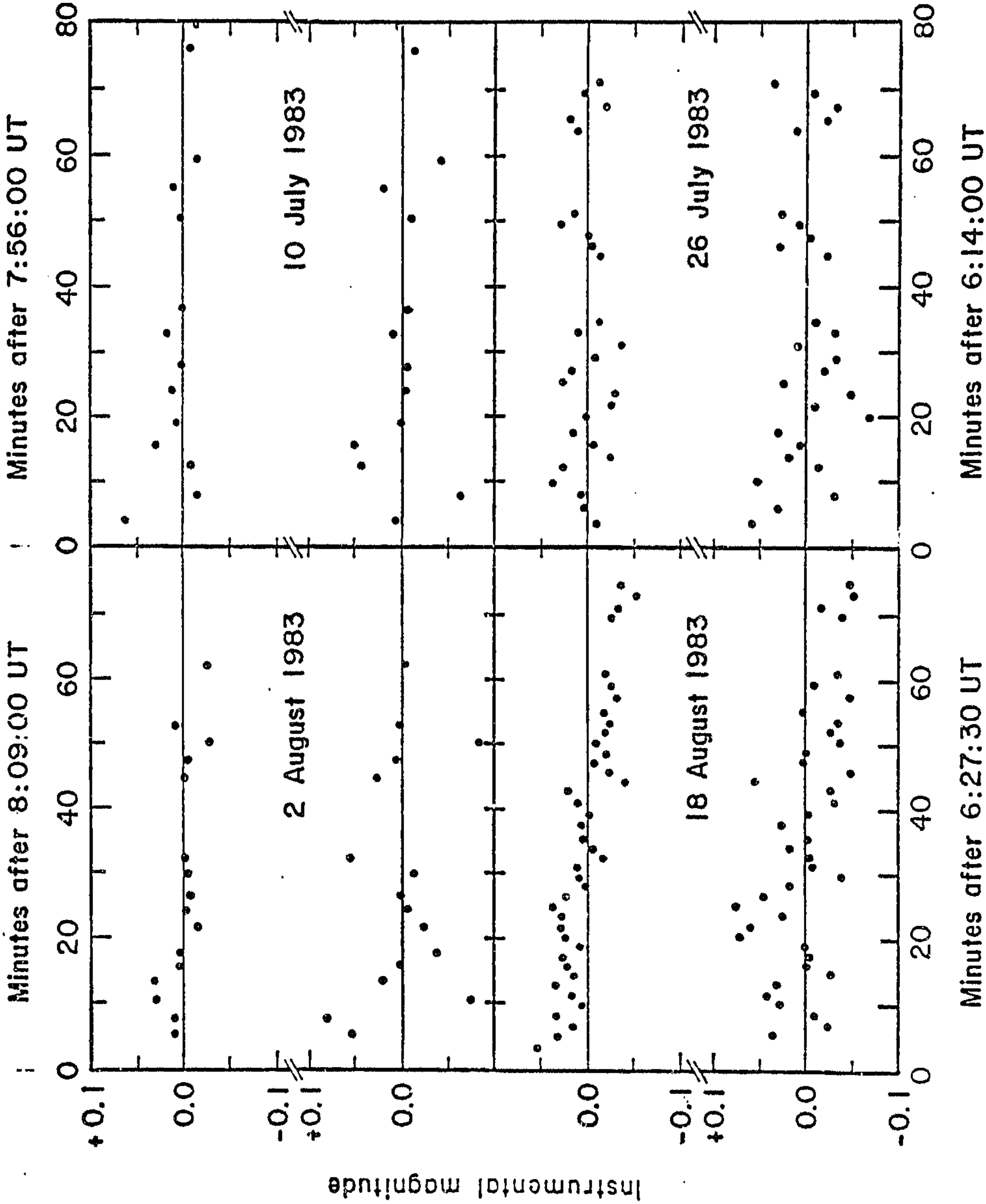
Minutes after 8:09:00 UT
Minutes after 7:56:00 UT
2 August 1983
10 July 1983
18 August 1983
26 July 1983
Minutes after 6:27:30 UT
Minutes after 6:14:00 UT
Instrumental magnitude
+0.1
0.0
-0.1
0
20
40
60
80

Fig. 13

probably a native component of the original icy surface concentrated in a thin, devolatilized regolith produced by the Phoebe-dust bombardment. Similar "ultracarbonaceous" material dominates the surfaces of the D-type asteroids, and may be the elusive non-ice component in the surfaces of other icy satellites. An Iapetus-like bombardment regime may be the cause of the large hemispheric asymmetry in regolith properties on Callisto.

Figure 14 shows the Iapetus spectrum with the contamination of water ice removed, and the best fit synthetic dark-side material spectrum.

12. Search for Outer Satellites of Saturn

Cruikshank used the 3.6-m CFH telescope in June 1984 in a search for outer, Phoebe-like satellites of Saturn. With the prime focus camera on 30 x 30 cm plates, each covering an unvignetted field of about 45 arcmin, six different fields were photographed to cover approximately 80% of the radius of action in which satellites might be expected. Several of the fields were photographed twice. The exposures were all 60 minutes long.

The red plates reached a depth of magnitude 23, and no satellites were found. Maximum sensitivity to satellite images was achieved by tracking the telescope at the Saturn rates, resulted in trailed star images but nontrailed images of satellites Iapetus and Phoebe.

The null result is significant because of the stringent limit it places on the existence of small Phoebe-like satellites in the region of Saturn's satellite space where captured objects might be found. For m_V = 23, the following satellite diameters correspond to the assumed geometric albedos listed:

Albedo (p_V)	0.03	0.05	0.10	0.20
Diameter (km)	15.6	12.0	8.4	6.0

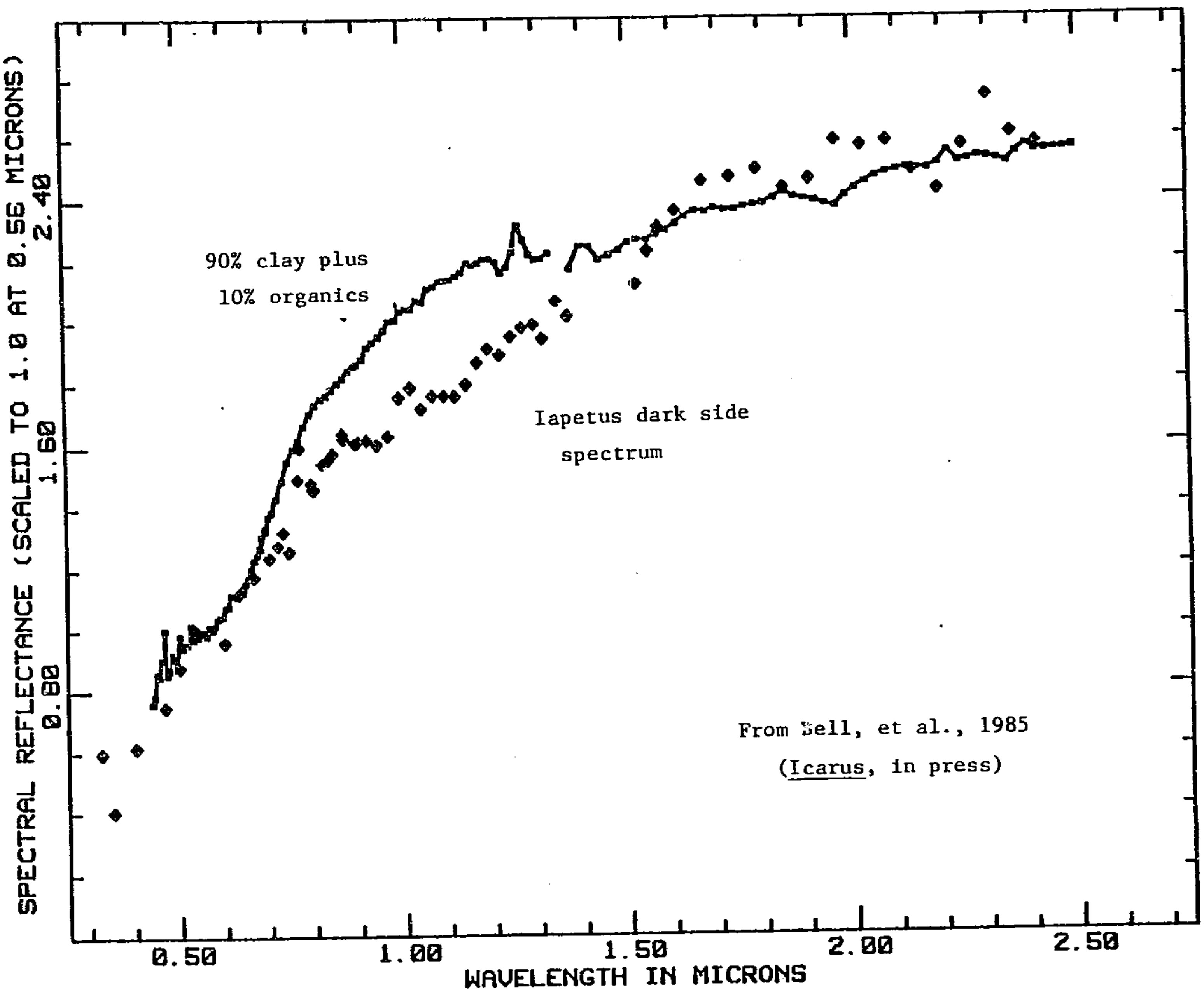

SPECTRAL REFLECTANCE (SCALED TO 1.0 AT 0.56 MICRONS)
0.80
1.60
2.40
90% clay plus
10% organics
Iapetus dark side
spectrum
From Bell, et al., 1985
(Icarus, in press)
0.50
1.00
1.50
2.00
2.50
WAVELENGTH IN MICRONS

Figure 14 -

By analogy with Phoebe, and in comparison with the small, captured satellites of Jupiter, we might expect exterior captured satellites of Saturn to have surfaces characterized by dark, carbonaceous material with albedo on the order of 3 or 5 percent. The new survey results indicate, then, that there are probably no satellites in the permitted space with diameters exceeding about 12 km.

13. Search for Outer Satellites of Uranus

During the search for outer satellites of Saturn (see above) made by Cruikshank with the CFH telescope, exposures of Uranus were also taken to approximately the same magnitude depth (about 23). The telescope was guided at the planetary rate to improve the chances of success in finding faint satellites, but none were found in the entire volume of space (defined by the radius of action) permitted. This upper limit to satellite size can be expressed in terms of assumed surface geometric albedo, as in the case of the discussion of satellites of Saturn, as follows:

Albedo (p_V)	0.03	0.10	0.20	0.40
Diameter (km)	72	40	38	20

Because the known satellites of Uranus are of relatively high albedo since they have strong ice signatures in their spectra, we might expect any undiscovered satellites to have similarly high albedos. Thus, the most probable upper limit to the diameters of any undiscovered satellites is probably on the order of 25–30 km.

D. ASTEROIDS AND COMETS

1. Modeling Asteroid Rotational Lightcurves

Goguen and K. Uchida, an undergraduate student employed during the summer, have written a program that numerically integrates the isotropic multiple scattering photometric function over the surface of a body of arbitrary shape producing the observable disk-integrated intensity. Rotation of the shape then yields a model lightcurve. This model lightcurve, using a triaxial ellipsoid body shape, will be fit by least squares to observed asteroid lightcurves obtained at a large range of orbital positions (e.g., the PSI photometric geodesy data) to determine axial ratios, pole orientations and surface photometric functions consistent with all available photometry. To accomplish this a least squares fitting program based on the Simplex algorithm, which requires only that the function being fit can be evaluated numerically, will be employed. The necessary software is written and tested, and application to observations has just begun.

2. Lightcurves of Trojan Asteroids

Goguen, Cruikshank, and Hartmann have obtained V photometry of Trojan asteroids 884, 1208, 2223, 2363, and 2893 to determine the rotation rates and lightcurve amplitudes. The goal of this study is to obtain a significant sample of rotation rates and lightcurve amplitudes to compare these aspects of the Trojan cloud asteroids to the main belt asteroids.

3. JHK Observations of Asteroids

The Arizona eight-color asteroid survey and Tholen's taxonomic classification of the asteroid spectra have identified several new classes of asteroids. In collaboration with E. F. Tedesco (JPL) and L. A. Lebofsky (U. Arizona), Tholen has been extending the spectra of asteroids representative of these new classes to JHK wavelengths using the IRTF. The results should help make mineralogical interpretations of the new classes easier, while also defining the color domains of these classes.

4. Near-earth Asteroids

Special attention continues to be given to near-earth asteroids whenever known ones become bright enough for physical observations, or when new ones are discovered. Two that fell into the latter category are 1984 KD and 1984 QA. Observations of the former at closest approach (when it was quite bright) were thwarted by cirrus; lower quality data were obtained later in the year when the object finally moved far enough north to once again be accessible from our latitude, although at a much fainter magnitude.

Object 1984 QA turned out to be quite a prize, being only the fifth known Aten-class asteroid to be discovered. In addition to the photometric data acquired (both visible from the 2.2-m and infrared from the IRTF), we used the excellent pointing characteristics of the IRTF to add a new dimension to our work: astrometry. The astrometric data obtained on 1984 QA proved to be crucial; we acquired the object on the basis of crude positions provided by E. F. Helin at Palomar and were the first to report accurate positions of the object, thus enabling other observers to acquire the object early in the apparition. We also obtained the last accurate positions of the object during that lunation, which enabled the most accurate possible orbit to be determined, simplifying the recovery of the object during the following lunation.

Emphasis was given to 1983 TB during its superb 1984 apparition. Object 1983 TB is the Apollo asteroid with an orbit coincident with the Geminid meteor stream. The coincidence of the orbits was the primary reason for believing that 1983 TB might be a comet. Extensive observations were obtained during December. The phase function was covered from 13 to 87°; the data will permit the scattering properties of the surface to be studied. Both visible and infrared colors were measured; the reflectance spectrum was found to be unique amont near-earth asteroids, resembling most closely the F-class asteroids found in the main belt. The visible photometry also yielded a lightcurve; preliminary analysis suggests an amplitude over 0.4 mag and a period slightly less than 4 hr, making 1983 TB one of the most rapidly rotating asteroids. No distinctly cometary attribute was found, however; yet it remains impossible to distinguish between the "asteroid" and "dead comet" possibilities. We can only say that 1983 TB is not an active comet. This conclusion was instrumental in the Minor Planet Center's decision to add 1983 TB to the catalog of numbered asteroids (number 3200).

Other near-earth asteroids observed in 1984 include 2100 Ra-Shalom, 3122 1981 ET3, and 3199 1982 RA. Ra-Shalom was targeted principally for lightcurve observations; an accurate period is needed for the proper interpretation of radar results obtained during its 1981 apparition by S. Ostro (JPL). Unfortunately, clouds interfered with observations during three different observing runs, virtually ruining any hope of improving the rotational period.

Object 1981 ET3 was successfully observed in December both at visual wavelengths using the 2.2 m and at infrared wavelengths using the IRTF. Preliminary analysis of the data show the object to be unusually red, possibly placing it in the rare A class of asteroids, whose spectra show the signature of relatively pure olivine.

Object 1982 RA became bright enough to observe with the Circular Variable Filter (CVF) at the IRTF. Its spectrum also shows the distinctive signature of relatively pure olivine, but in this case the absorption band appears to be saturated, suggesting that the surface of 1982 RA has rather large (~1 mm) grains of olivine on an iron substrate.

5. The Nature of C-class Asteroids

In collaboration with M. A. Feierberg (U. Maryland) and Lebofsky, Tholen investigated the correlation between the U-B color index and the strength of the water of hydration absorption feature seen in the spectra of several C asteroids at 3 μm. The results show a strong correlation, which is consistent with the theory that the lower temperatures which permit formation of hydrated minerals also promote higher oxidation states of iron in silicates (iron being responsible for the ultraviolet absorption feature in C asteroids which the U-B color index is sensitive to). The excellent correlation also suggests that the U-B color can be used as a powerful tool in mapping the presence of water in C asteroids, since UBV photometry can be applied to a much larger sample of objects than can 3 μm photometry. The results show that both hydrated and anhydrous objects coexist at the same heliocentric distances. The scenario developed for the evolution of C asteroids is that internal heating drove the water in initially homogenous bodies from the cores to the surfaces, leaving behind objects with anhydrous cores and surfaces that have undergone extensive aqueous alteration. Subsequent collisional fragmentation dispersed these objects, leaving behind the distribution of hydrated and anhydrous objects that we now observe.

6. Ceres Occultation

Tholen and Goguen attempted to observe the November 13 occultation by Ceres from the AF 24". Snow prevented the acquisition of any data, unfortunately. Analysis of mainland observations shows that the occultation path did pass over MKO.

7. Comet Halley Photometry

Photoelectric observations of Comet P/Halley at visible wavelengths were started by Tholen in December. Although the comet was not bright enough to be acquired visually, the ephemeris was accurate enough so that Halley could be easily located by blind offset techniques. Enough signal was present through a broadband blue filter to permit peaking on the signal. A preliminary reduction shows the late December blue magnitude of Halley to be 20.4, with slight evidence for some variability, although the data are insufficient to permit the confirmation of the large amplitude variation seen by other observers using CCD detectors.

8. Comet Halley Studies with the CCD

Cruikshank, in collaboration with C. R. Chapman (Planetary Science Institute, Tucson), obtained several CCD images of Comet Halley in October and November, 1984, using the 2.2-m telescope. The sky was not photometric, but Comet Halley and various other comets were observed in order to gain experience with the system and the data reduction routines. The purpose of the program is to obtain photometry of faint cometary nuclei with filters centered on continuum spectral regions. This will in principle give the reflectance of the nucleus in a spectral region (0.4-1.0 μm) where numerous asteroid and satellite data exist, thus permitting a direct comparison with results for well known objects. This program is continuing (data were obtained in photometric skies in February 1985). See Figures 15 and 16.

9. Distribution of Dust in the Inner Coma of Comet IRAS-Araki-Alcock (1983d)

Storrs participated in a study of this comet with A. T. Tokunaga, J. N. Heasley, and C. Christian (all of the Institute for Astronomy) using CCD images made at the 2.2-m telescope in May 1983. The Galileo/IfA CCD was used

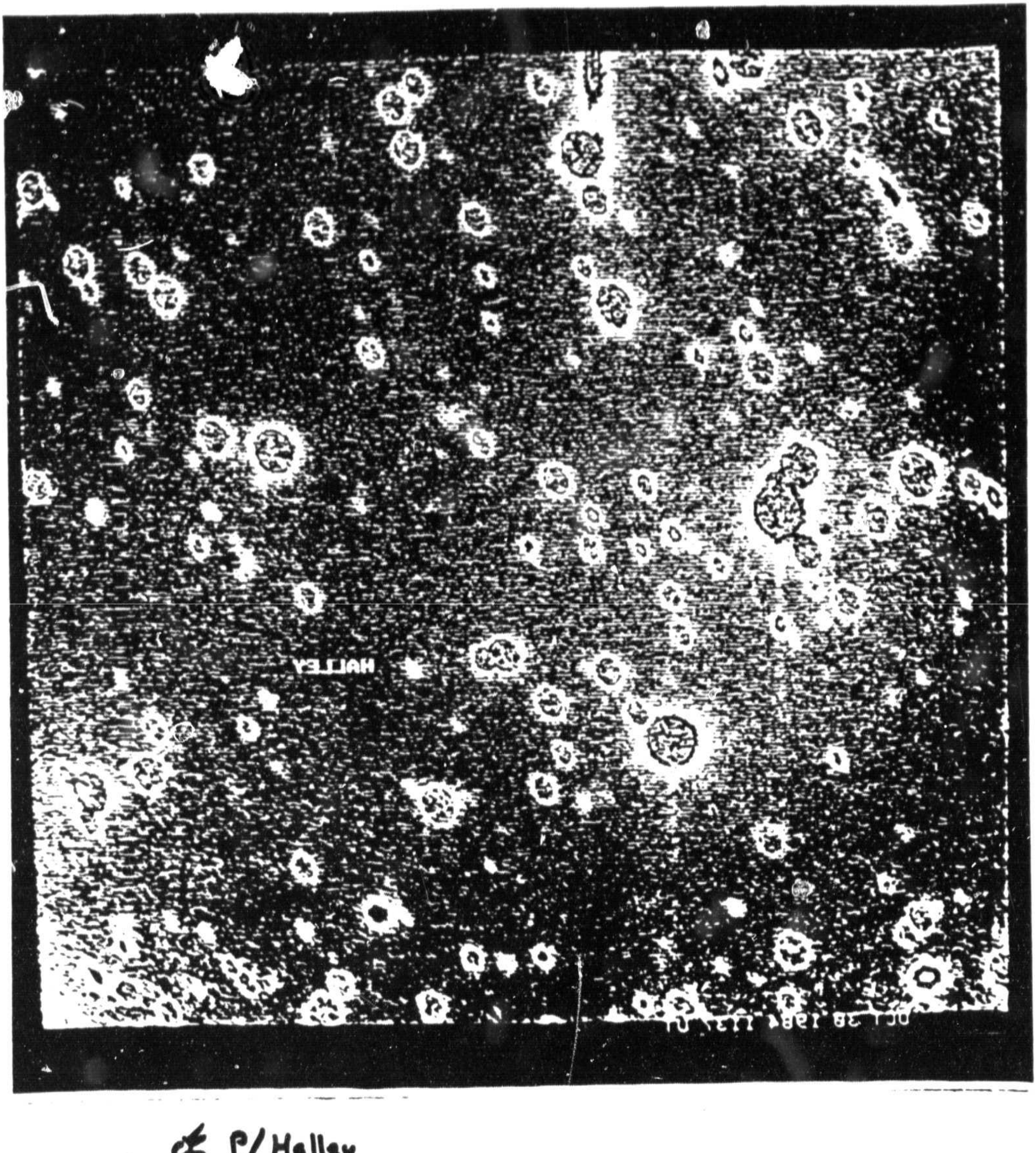

N
W
☌ P/Halley
1984 Oct 30.484
UH 88-inch

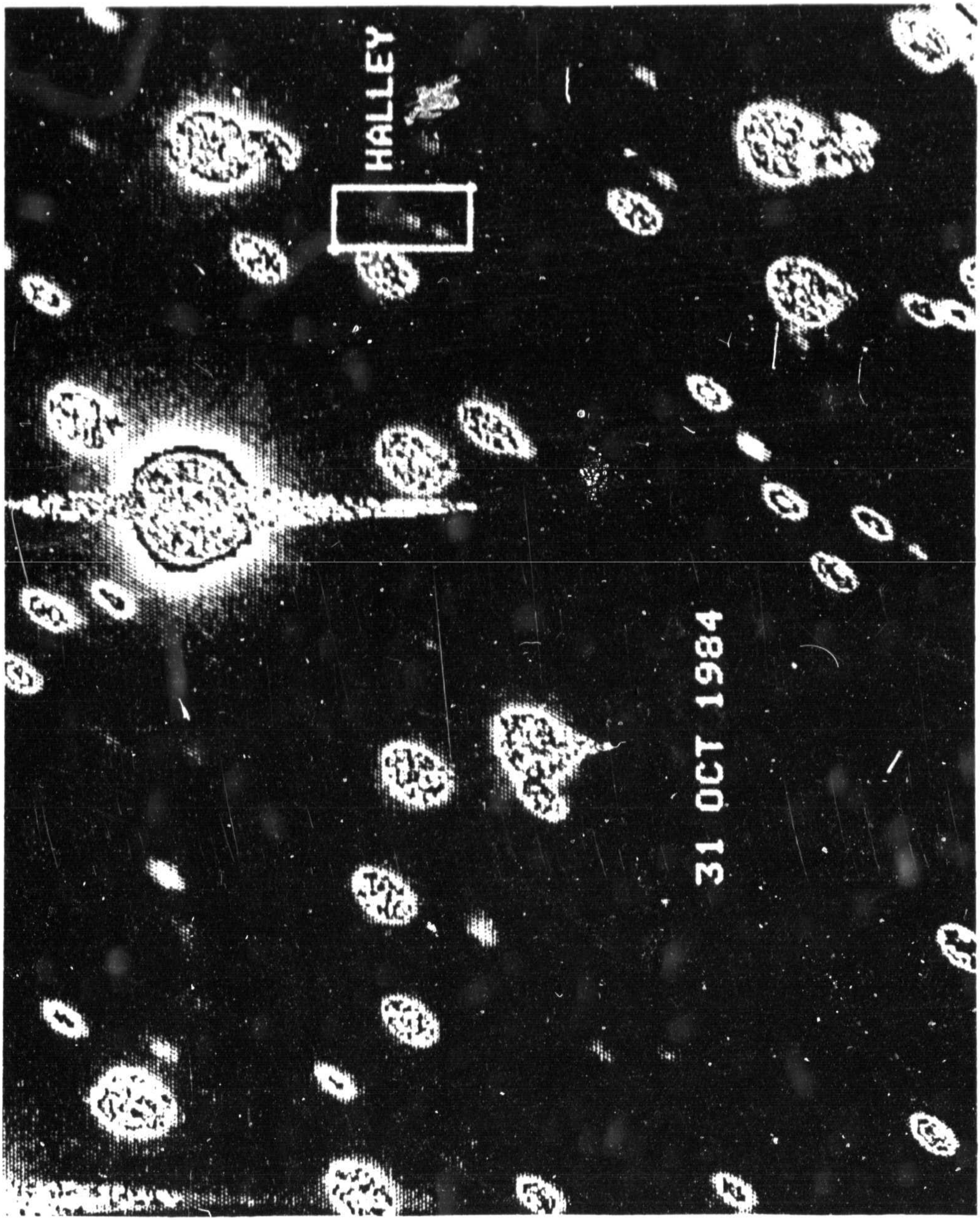
HALLEY
31 OCT 1984

on five nights, including the closest approach of the comet to the Earth. The images made on the day of closest approach (11 May) have spatial resolution of better than 20 km, making them the highest resolution comet images thus far obtained anywhere.

The data show a highly variable and asymmetric sunward emission in the coma of the comet, with a nearly stellar nucleus at its apex. Activity indicative of outbursts on the nucleus was seen in the images of 8, 11, and 12 May. The photometrically calibrated images were measured to determine the rate of fall-off of intensity at various positions in the inner coma. Complex and non-uniform outflow of dust is indicated from the variations observed. A power law of less than r^1 was found, suggesting that dust grains may fragment during outflow. Storrs and his colleagues also have considered other possibilities, such as the orbiting of dust grains or the episodic and irregular exhalation of dust clouds by the nucleus.

Storrs finds that the emission of dust from the nucleus was confined to the sunward direction. On the day of closest approach to the Earth, the comet had a point-like nuclear image of diameter less than 0.7 arcsec (corresponding to a nucleus of less than 17 km diameter). On this same day, a long filamentary structure was observed in the coma. If the curvature of the filament represents nuclear rotation, the outflow velocity was greater than about 0.1 km/sec from a highly collimated, localized hotspot on the nucleus.

The observed distribution of dust in the inner coma of comet 1983d did not conform to a simple, uniform model of the type established for other comets.

10. Infrared Measurements of the Temperature of Comet IRAS-Araki-Alcock (1983d)

Cruikshank and R. H. Brown (now at JPL) completed their study of the infrared photometry obtained of this comet.

Infrared (1.5-20 μm) observations of the nuclear condensation of the comet in the interval 5-8 May 1983 (UT) show the distribution of 3.5- to 20-μm radiation is blackbody in character with no evidence of 10 μm emission from silicate grains in the coma of the comet. The observed color temperature of the nuclear condensation comet was 319 ± 5 K on 7 May and 307 ± 5 K on 8 May. Low-resolution spectrophotometry in the 1.5- to 2.6-μm region shows no obvious emission or absorption features, but thermal radiation of approximately the same color temperature as the 3.5- to 20-μm radiation is present along with reflected sunlight. Scans of the nuclear region of the comet indicate that most of the thermal radiation observed at 11.6 and 20.0 μm came from an <60 km diameter, unrresolved area centered on the nuclear region. Absolute flux measurements suggest that cross-sectional areas of 70 km^2 and 40 km^2 were responsible for most of the thermal radiation from the nuclear condensation on 7 and 8 May, respectively.

Figures 17 and 18 show the photometric measurements with the blackbody fit. In each case, two fits are shown; one with high weight placed on the 20-μm point, and the other with the greatest weight placed on the two short wavelength points. The latter fit is the preferred one.

11. Outer Solar System Materials: Ices and Color Systematics

Cruikshank continued his collaboration with W. K. Hartmann and Tholen in the systematic observation of a number of small bodies in the outer solar system (OSS) with the techniques of VJHK photometry and CVF filter spectrophotometry. Both the 2.2-m telescope (for V photometry) and the IRTF

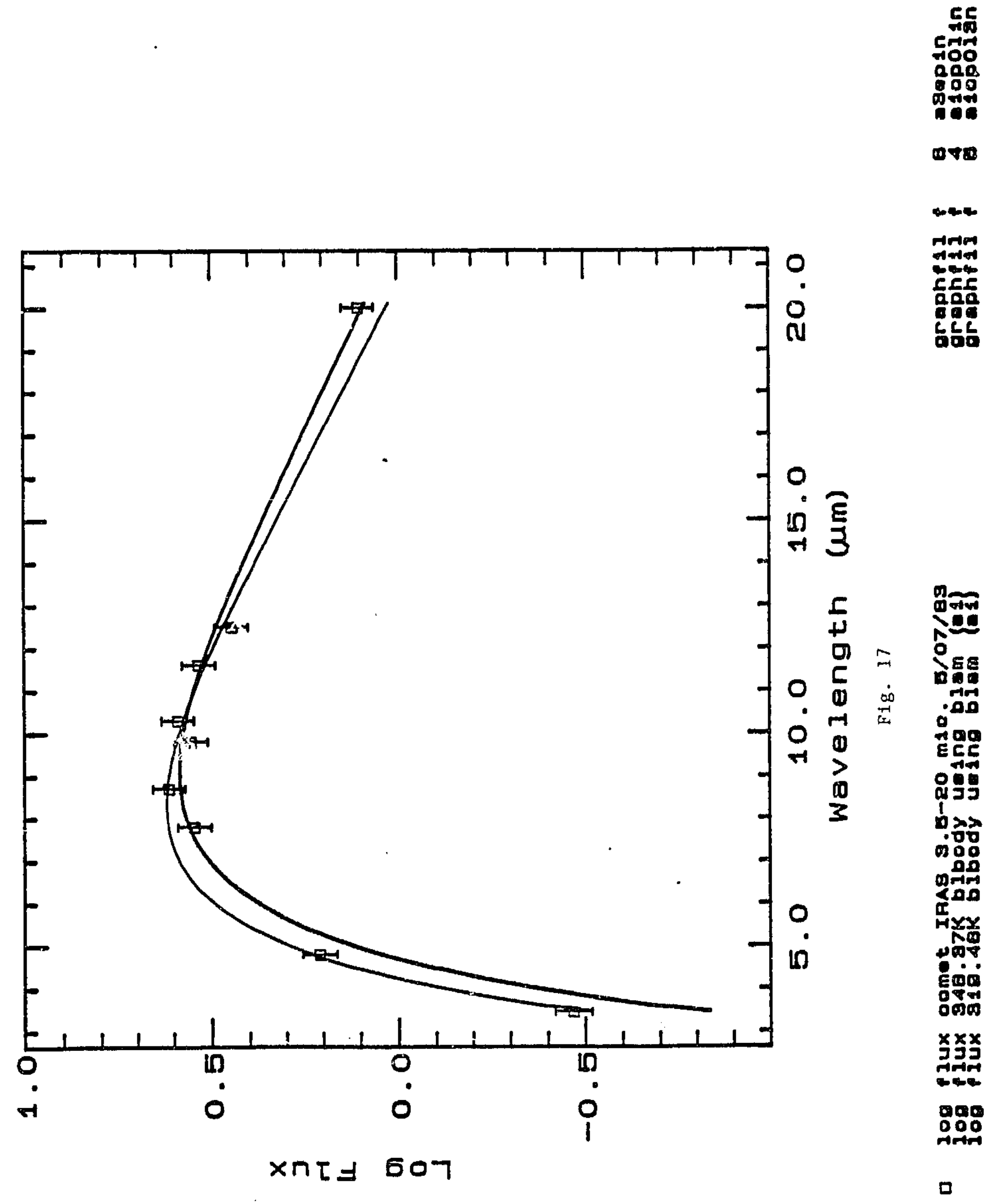
Log Flux
1.0
0.5
0.0
-0.5
Wavelength (μm)
5.0
10.0
15.0
20.0
log flux comet IRAS 3.5-20 mic. 5/07/83

Fig. 17

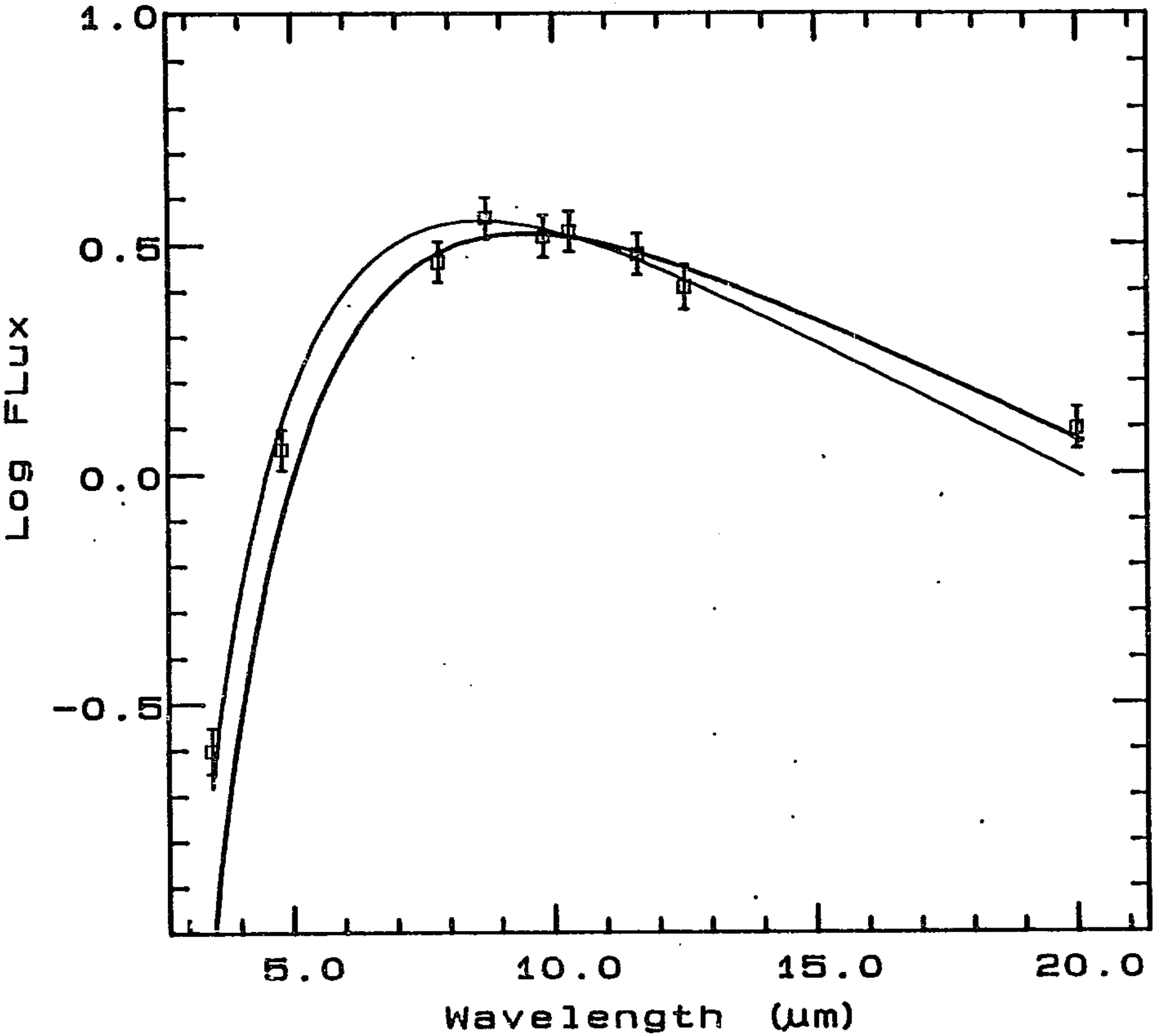

Fig. 18

□ log flux comet IRAS 3.5-20 mic. 5/08/83 graphfil f 8 a3epin
log flux 337.50K blbody using blam (ai) graphfil f 2 aiop01in
log flux 308.88K blbody using blam (ai) graphfil f 3 aiop013n

3-m telescope were used in this continuing work. The investigation began several years ago with J. Degewij as a colleague, but following Degewij's return to Europe and Tholen's joining the Institute staff, the latter has participated in the work. A review of the status of the work was given by Hartmann at the January 1984 meeting on Ices in the Solar System (NATO Conference) in Nice.

The project currently uses two runs per year on the IRTF, with simultaneous (when possible) observations of the same objects on the 2.2-m telescope. This permits us to work at maximum efficiency when getting VJHK photometry on solar system bodies too faint for observation with the low-resolution CVF (0.8–2.5 μm).

In this work, emphasis is placed on the relation of ices and solids in the OSS. Target objects include Trojan asteroids, outer-belt asteroids, comets, and small satellites. We have established correlations between VJHK colors and spectral classes among the brighter asteroids. We found a range of VJHK colors among OSS small bodies, from relatively bluer colors to relatively redder colors, with some clumping toward the two extremes, as shown in Figures 19 and 20. In all cases with measured albedo and known spectrum, the bluest objects have high albedo and spectrally ice-dominated surfaces, while the reddest objects have low albedos of only a few present surfaces classified in the C, D, and P asteroidal spectral classes. Ice is absent in the spectra of the latter, and their surfaces are spectrally dominated by dark carbonaceous soil.

VJHK colors (as opposed to JHK colors alone, obtained by most observers) are a remarkable tool for discriminating among OSS objects too faint for detailed spectrophotometry. Not only do ice-rich surfaces fall in a distinct field (lower left in both figures), but the C and D subtypes of dark materials

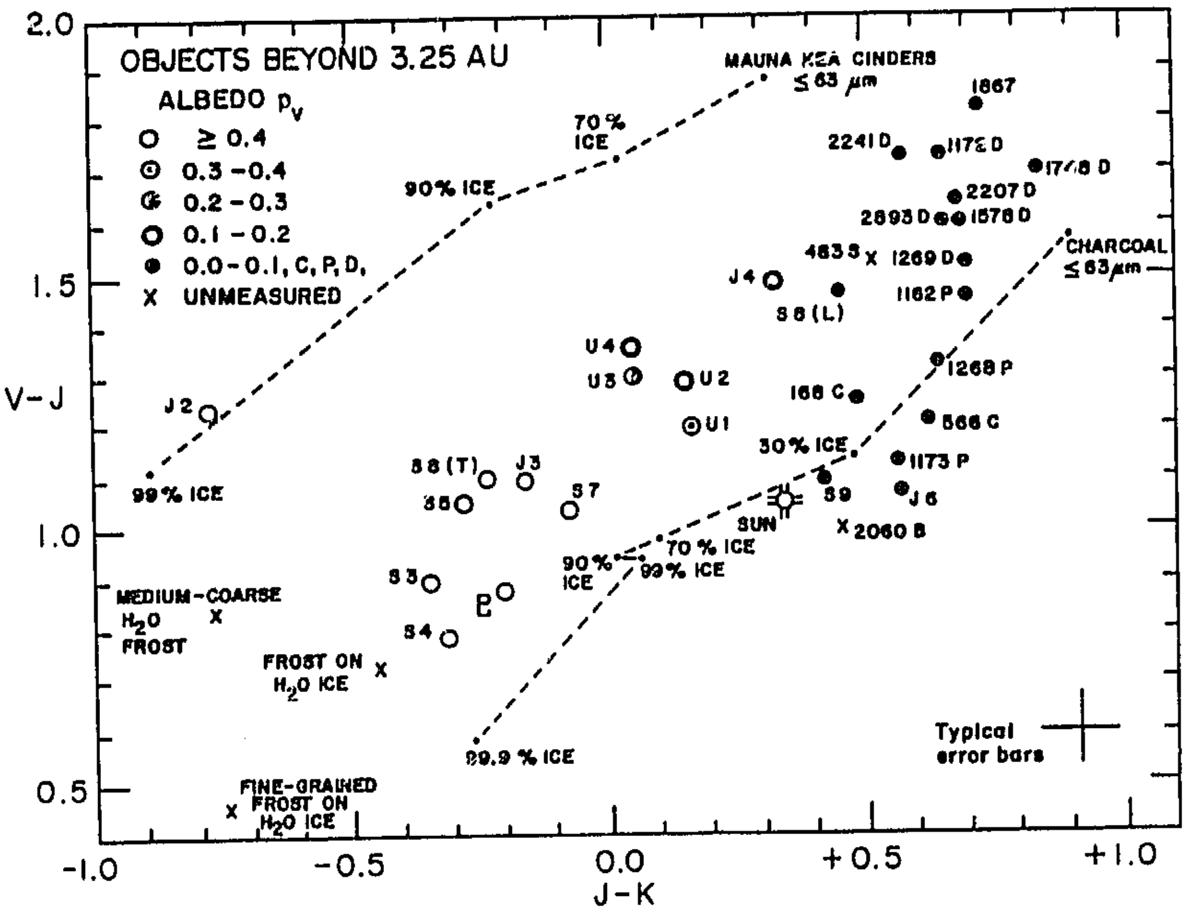

Figure 19. VJK color-color diagram for OSS objects (beyond the 2:1 Jupiter resonance at 3.25 A.U.). Albedos are indicated by symbols showing the progression from bright icy objects to dark surfaces. The fields of D-class asteroids (upper right) and C-class asteroids (right center) are well separated in JHK colors. Lab data on various forms of pure H_2O ice are in lower left. Dashed lines show "mixing tracks" defined by adding varying amounts of ice to soil samples.. "B" marks Chiron, designated as class "B" by Tholen.

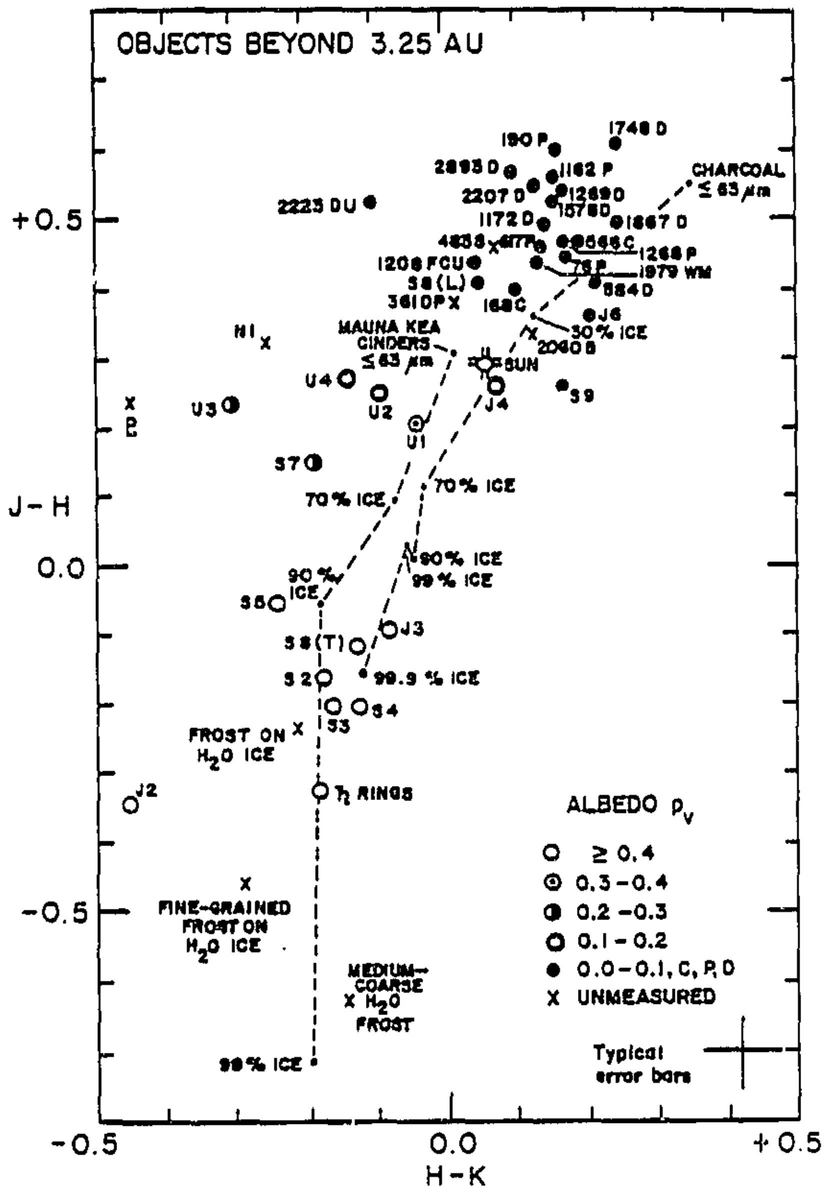

Figure 20. JHK color-color diagram for OSS objects. Diagram format is as in Figure 19. The progression of albedos, increasing strength of ice spectral bands toward lower left, and laboratory "mixing tracks" are all consistent with the hypothesis that many OSS surfaces are regolith mixtures of dark soils and bright ices, with mixing ratio a major factor in determining the spectrophotometric appearance.

are markedly segregated. The redder D-class (abundant among Trojans) is isolated in the upper right of VJH while the more neutral C's and P's (abundant in the outer belt) fall in the right center.

In summary, we have developed a working hypothesis relevant to ices in the OSS: most OSS surfaces can be represented, to first order, as two-component "salt and pepper" mixtures or bright ices and dark soils, whose ratios determine the spectral and colorimetric appearance. The soils may have different subtypes, including C, D, and P classes. Going a step further, Figure 19 suggests that surfaces such as seen on Rhea, Ganymede, Uranian satellites, Iapetus, and Callisto can be modeled by varying mixtures of D-type soils and ices. The C and P classes, together with outer (captured?) moons S9 Phoebe and J6 Himalia, may represent a suite of soils associated more closely with the outer belt than with the outermost solar system.

We have continued our observing program, emphasizing OSS objects and a search for ices. By observing VJHK colors of additional objects with known spectra in 1983 and 1984, we have improved our mapping of the C, D, and P fields over that reported in (7). Preliminary new data, insofar as reduced by us, are included in Figures 19 and 20, and were used to define the C, P, and D fields shown schematically in Figures 21 and 22. We anticipate a more complete data report in a separate paper.

We have obtained spectra of a number of these objects with circular variable filters (CVF's), ranging from 0.8 - 2.5 μm wavelength. Neither the colors nor the spectra give evidence of ice absorption bands in the surface materials, but as noted earlier, ices are easily masked by black soils in regoliths. We consider it possible, if not probable, that remote asteroids (e.g., D-class Trojans or Chiron) may have abundant ices in their surface or subsurface materials.

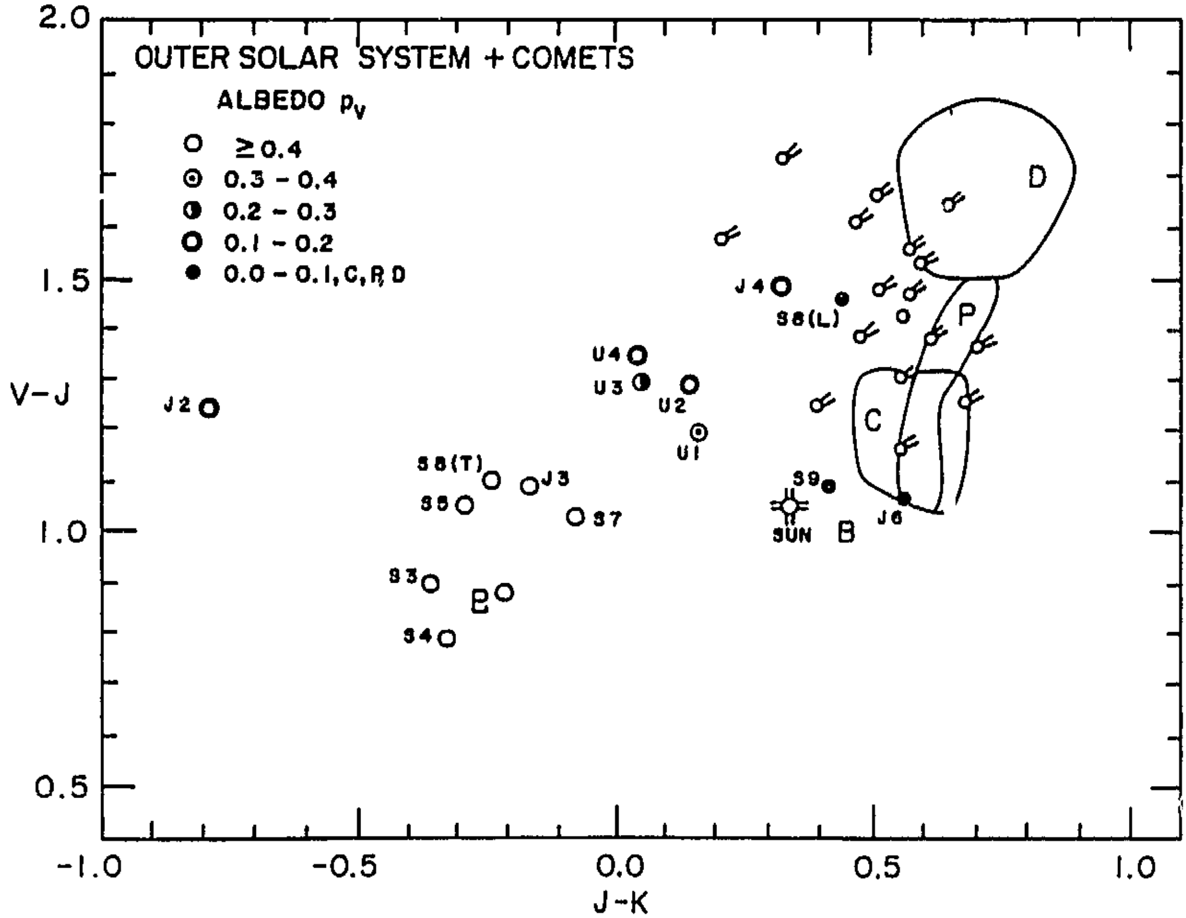

Figure 21. VJK data on comets, presented in the format of Figure 19. Comet data are from our own observations plus those of other observers as referenced in (7). C, P, and D asteroid fields are shown schematically based on our data for 6 C's, 5 P's, and 6 D's. Comet colors would be consistent with dirty ice materials colored by dark soils (esp. D-class soils) characteristic of OSS asteroids.

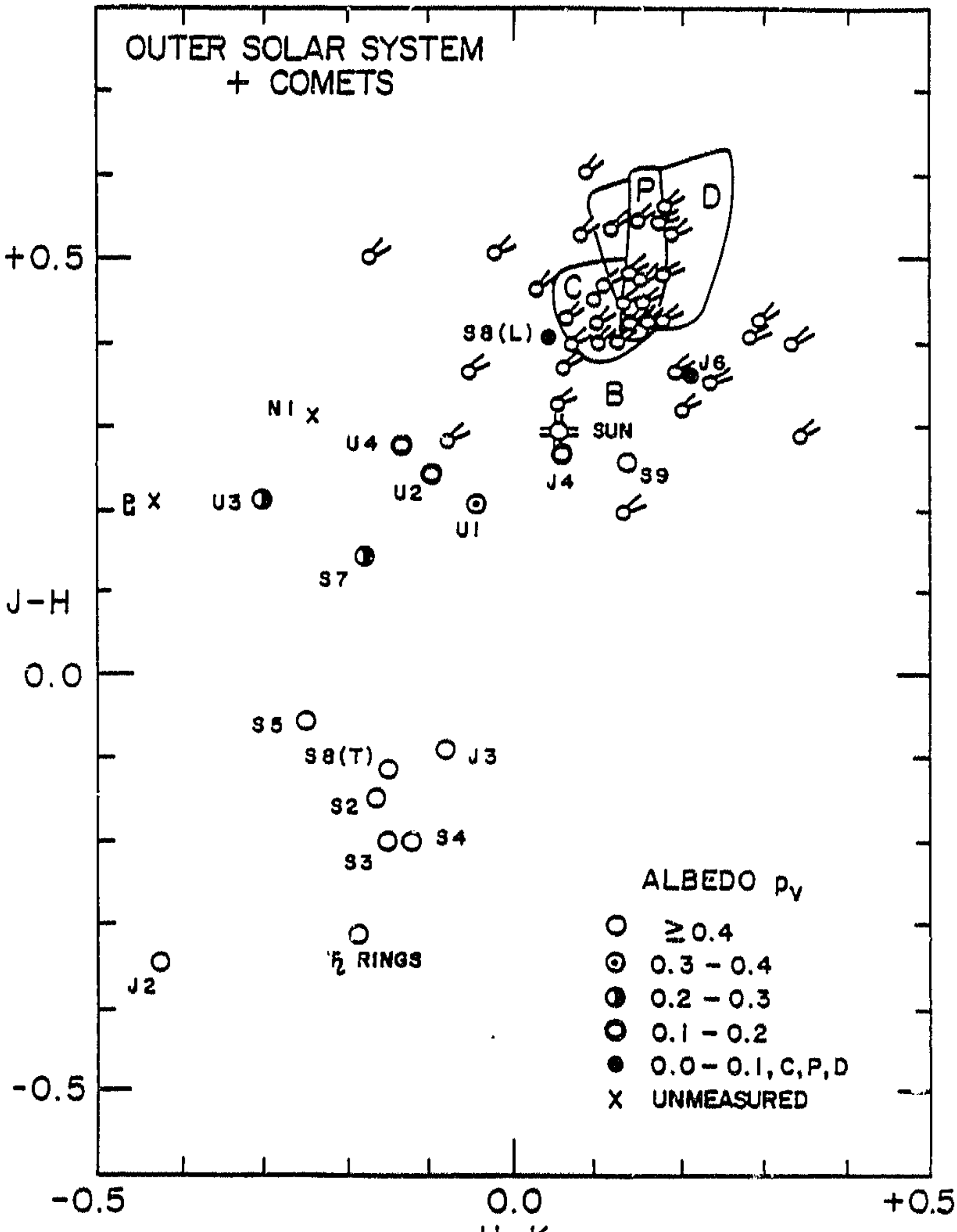

Figure 22. As in Figure 19, except using JHK data. IN JHK colors, the C, P, and D asteroid fields more nearly overlap. The fields were defined from our data for 7 C's, 6 P's, and 7 D's. Comets again are consistent with dirty ices colored by these soils, especially D soils. Several comets are too red (toward upper right) to involve C soils, and fall in the D field.

Having mapped the color fields of various OSS asteroids and small satellites, we have paid particular attention to comparisons with comets. Do comets (especially during low activity when far from the sun and too faint for spectra) match the colors of icy bodies, C asteroids, D asteroids, or Chiron? Or do they have unique colors? Such questions are complicated by the fact that we rarely, if ever, see the nuclear surfaces; observations are affected by scattering and phase effects of coma particles.

Nonetheless we have observed VJHK colors of comets at a wide range of phase angle and solar distance, emphasizing comets at large distance with minimal activity such as P/Schwassman-Wachmann 1 at 6 A.U. We found in all cases that comets lie near the D, P, and C class asteroid fields, as shown in Figures 21 and 22, in many cases offset toward the ice field. No comet revealed a color consistent with clean ice. The majority of the comets lie in a color field just offset from the D field. We concluded that the ices of comets are probably colored by dark dust similar to D-class asteroid material. This is in excellent agreement with the Gradie-Veverka prediction that comets contain D-type dust.

We also found that comet colors correlate with solar distance. The comets furthest from the sun, such as P/Schwassmann-Wachmann 1 (observed both during active outburst and quiescent phases) have colors most displaced from the D field toward the ice field. These resemble the colors of Clark's samples of black soil mixed with ice. Comets closer to the sun, however, at about 1-3 A.U., have VJHK colors most nearly matching D-class asteroids. Our proposed interpretation, consistent with current comet models, is that comet comas at >4 A.U. contain dirty ice grains colored by ice and dust, and that these grains have very long lifetimes at large solar distance. At smaller solar distances, the lifetime of the ice component in a grain is shorter, days or weeks at 2.3 A.U. but only an hour or less at 1 A.U. Therefore, among the closer, active comets, we see comas mostly composed of pure D-type dust, accounting for the D-like colors.

Obtaining 0.8 - 2.5 μm CVF spectra of a number of comets, including several remote examples, we hoped to obtain evidence of the water ice absorption bands near 2.0 and 2.4 μm. This would be an important result, since direct spectral detections of ice in comets have been marginal to date. Clean spectra of brighter comets near the sun show no evidence of these ice bands. Our results were limited by noise among faint distant comets, and while we found marginal suggestions of the ice bands in P/Schwassmann-Wachmann 1 and P/Bowell-Skiff, we are continuing the work in hopes of obtaining better data.

E. RELATED RESEARCH ACTIVITIES

1. Photometry of Solar Analog Stars and the Tie-in of Northern and Southern L' and M Standards

Sinton began an extension of the system of L' and M standards (Sinton and Tittemore 1984) to include more stars of dwarf type and to enable tying the Northern system with the Southern. Two categories of dwarf stars were added. The first are solar analog stars to enable a more accurate derivation of albedos of solar system objects. In this regard 61 Cyg B as well as other stars of nearly perfect spectral match to the sun are included. The second category of dwarf stars are very late cool dwarfs. Observations of these will enable other observers to make more accurate transformation to our system with the inclusion of color terms. At prsent it is not possible to tie observations of the late dwarfs to our system. The observation of late giants does not provide a satisfactory transformation for all stars because of the existence of luminosity dependent stellar absorption bands.

Standards from the AAO system (Allen, Mon. Not. Roy. Astr. Soc. 203, 777) are included to permit transformation between the two systems. At Mauna Kea we are in the unique position of being able to observe a sizable number of the Southern stars as well as all Northern stars. In particular, we are including BS3314, which is the Southern standard of zero color as α Lyr is for the Northern system.

The extension includes 34 stars, some as faint as 6.5 magnitude at M. About one-third of these were tied to the Sinton-Tittemore system of primary standards on at least 4 nights in 1984. The completion of the extension will require another year of observing in order to cover all parts of the sky. The system will then be comprised of 75 stars of all spectral types and reach as far south as -30°. Eighteen stars are south of the equator.

III. OTHER TOPICS

At the request of Institute Director Don Hall, Tholen has initiated a program to monitor the night sky brightness at MKO. The observations will be used to determine the dependence of the night sky brightness on ecliptic and galactic latitude, as well as on the location of man-made sources (principally the city of Hilo). Continued observations over the years will enable the natural and man-made contributions to the night sky brightness to be monitored, and in the case of the latter, controlled.

Cruikshank participated in a NATO workshop, "Ices in the Solar System", in Nice, France, January 1984, where he gave two contributed and one invited talk.

Cruikshank gave invited colloquia at Stony Brook, Goddard Space Flight Center (both in January 1984) and at California Institute of Technology (February 1984).

Cruikshank participated in a Voyager workshop on Uranus and Neptune sponsored by JPL in February 1984, where he gave one invited and one contributed talk.

Tholen has continued his participation in the IRAS Asteroid Workshops held at Jet Propulsion Laboratory.

Morrison continues to chair the Solar System Exploration Management Council.

Cruikshank and Morrison continue as Associate Editors of Icarus.

IV. BOOKS AND PAPERS PUBLISHED OR SUBMITTED IN 1984

A. PUBLISHED

D. E. Backman, E. E. Becklin, D. P. Cruikshank, R. R. Joyce, T. Simon, and A. Tokunaga. Infrared Observations of the Eclipse of Epsilon Aurigae: Direct Measurement on the 500 K Secondary at 5, 10, and 20 Microns. Astrophys. J. 284:799-805, 1984.

R. H. Brown and D. Morrison. Diameters and Albedos of Thirty-six Asteroids. Icarus 59:20-24, 1984.

D. P. Cruikshank. Physical Properties of the Satellites of Neptune. Uranus and Neptune. NASA Conference Publication 2330, pp. 425-436, 1984.

D. P. Cruikshank. Variability of Neptune. Uranus and Neptune. NASA Conference Publication 2330, pp. 279-287, 1984.

D. P. Cruikshank, and J. Apt. Methane on Triton: Physical State and Distribution. Icarus 58:306-311, 1984.

D. P. Cruikshank, and R. H. Brown. The Nucleus of Comet P/Schwassmann-Wachmann 1. Icarus 56:377-380, 1984.

D. P. Cruikshank, R. H. Brown, and R. N. Clark. Nitrogen on Triton. Icarus 58:293-305, 1984.

D. P. Cruikshank, and W. K. Hartmann. The Meteorite-Asteroid Connection: Two Olivine Asteroids. Science 223:281-283, 1984.

W. K. Hartmann, and D. P. Cruikshank. Comet Color Changes with Solar Distance. Icarus 57:55-62, 1984.

J. N. Heasley, C. B. Pilcher, R. R. Howell, and J. C. Caldwell. Restored Methane Band Images of Uranus and Neptune. Icarus 57:432-442, 1984.

R. J. Hlivak, J. P. Henry, and C. B. Pilcher. Experience with 800 x 800 Virtual Phase and 500 x 500 Three-Phase CCD Imagers. In Instrumentation in Astronomy V, SPIE Proceedings 445:122-127, 1984.

R. R. Howell, D. P. Cruikshank, and F. P. Fanale. Sulfur Dioxide on Io: Spatial Distribution and Physical State. Icarus 57:83-92, 1984.

L. A. Lebofsky, D. J. Tholen, G. H. Rieke, and M. J. Lebofsky. 2060 Chiron: Visual and Thermal Infrared Observations. Icarus 60:532-537, 1984.

J. S. Morgan, S. C. Wolff, S. E. Strom, and K. M. Strom. Narrow-band Imaging and Velocity Maps of Young Stellar Objects: Initial Results. Astrophys. J. Lett. 285:L71-L73, 1984.

D. Morrison, T. Johnson, E. Shoemaker, L. Soderblom, B. Smith, P. Thomas, and J. Veverka. Saturn Satellites: Geological Perspective. In Saturn (T. Gehrels and M. S. Matthews, Eds.). Tucson: University of Arizona Press, pp. 609-639, 1984.

C. B. Pilcher, W. W. Smyth, M. R. Combi, and J. H. Fertel. Io's Sodium Directional Features: Evidence for a Magnetospheric-Wind-Driven Gas Escape Mechanism. Astrophys. J. 287:427-444, 1984.

E. J. Shaya, and C. B. Pilcher. Polar Cap Formation on Ganymede. Icarus 58:74-80, 1984.

W. M. Sinton, J. Goguen, and R. Howell. Jupiter I, Io (Eruption of Loki Volcano). Internat. Astron. Union Circ. No. 3962, 1984.

W. M. Sinton, and W. C. Tittemore. Photometric Standard Stars for L' and M Filter Bands. Astron. J. 88:1366-1370, 1984.

D. Tholen. Observations Made at Mauna Kea by D. Tholen. Minor Planet Circ. 9142, 1984.

D. Tholen. Observation Made at Mauna Kea by D. Tholen. Minor Planet Circ. 9266, 1984.

D. Tholen, D. Cruikshank, and W. Hartmann. Observations Made at Mauna Kea by Minor Planet Circ. 9053, 1984.

D. Tholen, and B. Zellner. Multi-color Photometry of Outer Jovian Satellites. Icarus 58:246-253, 1984.

B. SUBMITTED OR IN PRESS

J. F. Bell, D. P. Cruikshank, and M. J. Gaffey. The Composition and Origin of the Iapetus Dark Material. Icarus (in press), 1985.

R. H. Brown, D. P. Cruikshank, and D. Griep. Temperature of Comet 1983d (IRAS-Araki-Alcock). Icarus (in press), 1985.

J. Burns, and D. Morrison. Introduction to the Satellites. In Natural Satellites (J. Burns and D. Morrison, Eds.). Tucson: University of Arizona Press (in press), 1985.

J. Burns, and D. Morrison, Eds. Natural Satellites. Tucson: University of Arizona Press (in press), 1985.

D. P. Cruikshank. The Small, Icy Satellites of Saturn. In Ices in the Solar System, Proceedings NATO Workshop, Nice, January 1984 (J. Klinger and A. Dollfus, Eds.) (in press), 1985.

D. P. Cruikshank, and R. H. Brown. Outer Planet Satellites. In Natural Satellites (J. A. Burns and D. Morrison, Eds.). Tucson: University of Arizona (in press), 1985.

D. P. Cruikshank, R. H. Brown, and R. N. Clark. Methane Ice on Triton and Pluto. In Ices in the Solar System, Proceedings NATO Workshop, Nice, January 1984 (J. Klinger and A. Dollfus, Eds.) (in press), 1985.

D. P. Cruikshank, W. B. Hartmann, and D. J. Tholen. Comet Halley: Color, Albedo, and Size of the Nucleus. Nature (submitted), 1985.

D. P. Cruikshank, R. R. Howell, T. R. Geballe, and F. P. Fanale. Sulfur Dioxide Ice on Io. In Ices in the Solar System, Proceedings NATO Workshop, Nice, January 1984 (J. Klinger and A. Dollfus, Eds.) (in press), 1985.

M. A. Feierberg, L. A. Lebofsky, and D. J. Tholen. The Nature of C-class Asteroids from 3.0-micron Spectrophotometry. Icarus (submitted), 1984.

J. Goguen, H. B. Hammel, and R. H. Brown. V Photometry of Titania, Oberon, and Triton. Icarus (submitted), 1984.

J. Goguen, and J. Veverka. The Isotropic Multiple Scattering Approximation: Its Consequences and Application to Planetary Photometry. Icarus (submitted), 1984.

H. B. Hammel, J. D. Goguen, W. M. Sinton, and D. P. Cruikshank. Observational Tests for Sulfur Allotropes on Io. Icarus (submitted), 1984.

W. K. Hartmann, and D. P. Cruikshank. Asteroid and Comet Studies in the Near Infrared. In Ices in the Solar System, Proceedings NATO Workshop, Nice, January 1984 (J. Klinger and A. Dollfus, Eds.) (in press), 1985.

R. R. Howell, D. P. Cruikshank, and T. R. Geballe. The Plumes of Io: A Detection of Solid Sulfur Dioxide Particles. Science (submitted), 1985.

W. B. Hubbard, et al. (including D. Tholen). Results from Observations of the 15 June 1983 Occultation by the Neptune System. Astron. J. (in press), 1985.

T. V. Johnson, D. Morrison, D. L. Matson, G. J. Veeder, R. H. Brown, and R. M. Nelson. Io Volcanic Hot Spots: Stability and Longitudinal Distribution, Science (in press), 1984.

J. S. Morgan. Images of the Io Torus. Sky and Telescope (in press), 1984.

J. S. Morgan. Models of the Io Torus. Icarus (submitted), 1984.

J. S. Morgan. Temporal and Spatial Variations in the Io Torus. Icarus (submitted), 1984.

C. B. Pilcher, and J. S. Morgan. Magnetic longitude variations in the Io torus. Advances in Space Research (in press), 1984.

C. B. Pilcher, J. H. Fertel, and J. S. Morgan. [S II] Images of the Io Torus. Astrophys. J. 291 (in press), 1985.

F. Pilcher, R. P. Binzel, and D. J. Tholen. Rotations of 1168 Brandia and 1219 Britta. Minor Plant Bull. (in press), 1985.

L. A. Soderblom and D. Morrison. Saturn Satellite System. In Natural Satellites (J. Burns and D. Morrison, Eds.). Tucson: University of Arizona Press (in press), 1985.

END

DATE

FILMED

JUN 7 1985